European Journal of Medicinal Chemistry 190 (2020) 112111

Contents lists available at ScienceDirect

European Journal of Medicinal Chemistry

journal homepage: http://www.elsevier.com/locate/ejmech

Research paper

Design, synthesis and biological evaluation of novel 2-(5-aryl-1*H*-imidazol-1-yl) derivatives as potential inhibitors of the HIV-1 Vpu and host BST-2 protein interaction

Thompho J. Rashamuse [a, b], Zikhona Njengele [a, c], E. Mabel Coyanis [a], Yasien Sayed [c], Salerwe Mosebi [d, **], Moira L. Bode [b, *]

[a] Centre for Metal-based Drug Discovery, Advanced Materials Division, Mintek, 200 Malibongwe Drive, Randburg, 2125, South Africa
[b] Molecular Sciences Institute, School of Chemistry, University of the Witwatersrand, Private Bag 3, PO WITS, 2050, South Africa
[c] Protein Structure-Function Research Unit, School of Molecular and Cell Biology, University of the Witwatersrand, Johannesburg, 2050, South Africa
[d] Department of Life and Consumer Sciences, College of Agriculture and Environmental Sciences, University of South Africa, Private Bag X6, Florida, 1710, South Africa

ARTICLE INFO

Article history:
Received 29 November 2019
Received in revised form
17 January 2020
Accepted 31 January 2020
Available online 4 February 2020

Keywords:
TosMIC
2-(5-aryl-1*H*-imidazol-1-yl)
HIV-1 Vpu
BST-2
ELISA
AlphaScreen assay

ABSTRACT

Novel ethyl 2-(5-aryl-1*H*-imidazol-1-yl)-acetates **17** and propionates **18**, together with their acetic acid **19** and acetohydrazide **20** derivatives, were designed and synthesized using TosMIC chemistry. Biological evaluation of these newly synthesized scaffolds in the HIV-1 Vpu- Host BST-2 ELISA assay identified seven hits (**17a**, **17b**, **17c**, **17g**, **18a**, **20f** and **20g**) with greater than 50% inhibitory activity. These hits were validated in the HIV-1 Vpu- Host BST-2 AlphaScreen™ and six of the seven compounds were found to have comparable percentage inhibitory activities to those of the ELISA assay. Compounds **17b** and **20g**, with consistent percentage inhibitory activities across the two assays, had IC_{50} values of 11.6 ± 1.1 μM and 17.6 ± 0.9 μM in a dose response AlphaScreen™ assay. In a cell-based HIV-1 antiviral assay, compound **17b** exhibited an EC_{50} = 6.3 ± 0.7 μM at non-toxic concentrations (CC_{50} = 184.5 ± 0.8 μM), whereas compound **20g** displayed antiviral activity roughly equivalent to its toxicity (CC_{50} = 159.5 ± 0.9 μM). This data suggests that compound **17b**, active in both cell-based and biochemical assays, provides a good starting point for the design of possible lead compounds for prevention of HIV-1 Vpu and host BST-2 protein binding in new anti-HIV therapeutics.

1. Introduction

The human immunodeficiency virus type 1 (HIV-1) therapy or treatment has been effective in changing the once acute fatal disease into a chronic and manageable condition. Nevertheless, the evolution of prevailing strains has led to multiple drug-resistance against current Food and Drug Administration (FDA) approved antiretroviral compounds [1–3]. This highlights the need in HIV-1 research to continue the search for new therapeutic targets. Recent HIV research efforts have focused on the development of small molecules that can target interactions between the HIV-1 proteins and the host proteins essential for viral replication [4–6]. Viral - host cofactor interactions could offer plausible alternative targets for therapeutic intervention [4–6]. One such interaction, that between the host bone marrow stromal cell antigen 2 (BST-2) and the HIV-1 Viral protein U (Vpu) has attracted significant attention as a new approach for the development of next-generation anti-HIV-1 treatment [7–9].

BST-2 (also known as tetherin, CD317, or HM1.24) is a type II transmembrane protein 180 amino acids long. This interferon inducible (α-IFN) host restriction factor bears a short cytoplasmic *N*-terminal tail region (CT) of 21 amino acids, an alpha (α)-helical transmembrane domain (TM) of 21 amino acids, a central coil-coiled extracellular domain (EC) of 116 amino acids and a C-terminal glycosylphosphatidylinositol (GPI) domain. The TM α-helical structure serves as an anchor of the protein to the plasma membrane while GPI, which forms part of the C-terminal domain, acts as a secondary anchor connecting the BST-2 back to the cell membrane [7–13]. Both TM and GPI anchors of BST-2 are essential for

* Corresponding author.
** Corresponding author.
E-mail addresses: mosebs@unisa.ac.za (S. Mosebi), Moira.Bode@wits.ac.za (M.L. Bode).

https://doi.org/10.1016/j.ejmech.2020.112111
0223-5234/

restriction of virus release. The EC domain provides dimer stability through the formation of a disulfide bond between cysteine residues, which is necessary for retention of antiviral activity [7–13].

HIV-1 Vpu is a type I integral protein of 81 amino acids and is one of four accessory genes encoded in HIV-1 [14–17]. HIV-1 Vpu consists of a hydrophobic *N*-terminal domain in the transmembrane region, which has a well-defined α-helix structure, and a hydrophilic C-terminal domain residing in the cytoplasmic region which consists of two α-helical domains linked together by two phosphorylated serine residues [18,19]. Phosphorylation of the two serine residues in Vpu is mediated by casein kinase II enzyme [17]. The typical functions of Vpu in viral replication include virion assembly, $CD4^+$ degradation and enhancement of extracellular viral particles [15,20,21]. Although the exact mechanism involved in the HIV-1 Vpu-mediated downregulation of BST-2 is not fully explained, current data proposes numerous possible mechanistic actions; i.e. degradation, cell-surface downregulation and trafficking alteration which results in intracellular sequestration of BST-2 within the endomembrane system [7,22–24]. Detailed mutagenesis studies have shown that interactions between amino acids Ala10, Ala14, Ala18 and Trp22 of Vpu and the following amino acids: Val30, Ile33, Ile34, leu37, Leu41 and Thr45 of BST-2 protein (Fig. 1) are essential for sustaining the downregulation of $CD4^+$, while at the same time enabling budding and enhancing the release of new virions [25–28].

To date, two peptides, BST-2-TM-P1 and BST-2-TM-P1-MT, have been described to inhibit the binding of the HIV-1 Vpu protein to the host BST-2 protein [29]. However, these peptide inhibitors suffered setbacks in their development: they have molecular sizes greater than 4000 g/mol and anti-HIV effects that can only be achieved at higher doses [29]. In contrast, several small molecules have been identified that can restrict the role of the HIV-1 Vpu protein. These include BIT-225 (**1**), currently in clinical trials, IMB-LA (**2**), 2-thio-6-azauridine (**3**); HMA (**4**); SM111 (**5**) and SM113 (**6**) (Fig. 2) [30–33]. These molecules have been found to specifically target the Vpu viroporin function, ultimately inhibiting HIV-1 particle release and impairing virion infectivity. Although these compounds do not necessarily prevent the interaction between BST-2 and Vpu proteins, they offer the proof of concept that small heterocyclic compounds can be developed to block the antagonist function of HIV-1 Vpu and thus expose HIV-1 to restriction by BST-2.

Over the last two decades, amino acid-based drug design has been the subject of great interest in the pharmaceutical and agrochemical industries [34–36]. Utilization of natural amino acids as building blocks has proven to be useful for the modern drug discovery platform because of their functional versatility and structural variety [34–36]. They signify a nearly limitless range of various structural features for the design and development of new therapeutic drugs [37,38]. Thus, exploration of more efficient and general protocols to access functionalized amino acids for therapeutic purposes is of great importance [38–40].

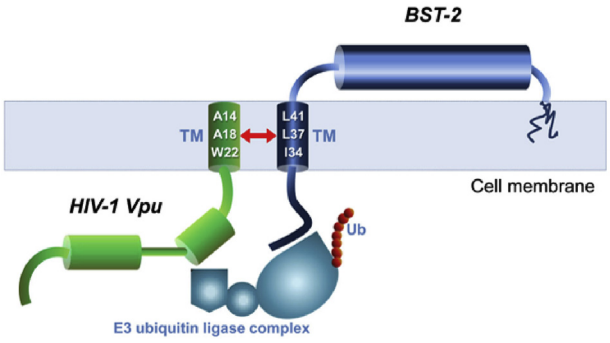

Fig. 1. Representation of the interaction of HIV-1 Vpu and BST-2 through their transmembrane domains [adapted from Arias, Iwabu and Tokunaga, ref. 11].

On the other hand, compounds containing imidazole as the central core exhibit a wide variety of biological properties, such as anti-fungal [41,42], anti-HIV [43,44], anti-microbial [45,46] and anti-cancer properties [47], and, therefore, the synthesis of imidazole-containing compounds remains relevant in medicinal chemistry.

A number of divergent building blocks have been exploited to efficiently access *N*-containing heterocyclic scaffolds, including isocyanide synthons. *Para*-toluenesulfonylmethyl isocyanide (TosMIC **7**) is a valuable synthetic building block in the preparation of several nitrogen containing heterocyclic compounds [48–50]. This synthon consists of a sulfonyl substituent, two *alpha* (α) - acidic protons and an isocyano reaction site (Fig. 2). These various functionalities result in exceptional reaction diversity and broad synthetic potential for the synthon.

The incorporation of amino acids into nitrogen (*N*)-containing heterocyclic compounds has been shown to positively contribute to the development of new biologically active molecules [51–54]. This combination improves the drug resistance abilities and enhances the pharmacological properties of the molecules [51–54]. Thus, the synthesis of *N*-heterocycle-based amino acid scaffolds presents an attractive approach for the development of new therapeutic agents in medicinal chemistry. Indeed, a number of the *N*-heterocycle-based amino acid inhibitors have been utilised in various therapeutic areas due to their ability to transport bioactive compounds through cellular membranes [51–54]. Hence, our rationale was that a combination of the imidazole core with a simple amino acid structure might serve as a starting point for the identification of valuable hit compounds that could then be elaborated into possible inhibitors specifically targeting the Vpu - BST-2 transmembrane interaction.

With the above facts in mind and our interest in TosMIC chemistry [55,56], we were encouraged to integrate two moieties to access small libraries of 2-(5-aryl-1*H*-imidazol-1-yl)-based compounds that were subsequently evaluated for their inhibitory activity against the HIV-1 Vpu and BST-2 protein interaction.

2. Results and discussion

2.1. Chemistry

The targeted 2-(5-aryl-1*H*-imidazol-1-yl) scaffolds consisting of acyl, carboxylic acid and acetohydrazide functionalities were efficiently synthesized by the route illustrated in Scheme 1. Initially, natural amino acids, glycine **8** and L-alanine **9**, were converted to the corresponding amino acid ethyl ester hydrochloride salts **10** and **11** in the presence of $SOCl_2$ in ethanol, followed by treatment with Et_3N in $CHCl_3$ to afford free amino esters **12** and **13** [57–59]. These amino esters were further subjected to a condensation reaction with various benzaldehydes **14a-g** in DCM in the presence of $MgSO_4$ at room temperature for 16 h to produce the ethyl 2-(arylideneamino)acyl intermediates **15** and **16** [57–59]. These intermediates were allowed to react with TosMIC **7** in the presence of DBU in DCM at room temperature for 24 h, followed (after solvent removal) by microwave irradiation in toluene at a set temperature of 115 °C for 10 min to afford a series of novel ethyl 2-(5-aryl-1*H*-imidazol-1-yl)acetates **17** and propionates **18** in various yields (Table 1). The substituents on the aryl ring had a strong influence on the yields of the products. Moreover, the presence of a stereogenic centre in compounds **16a-c** had a strongly negative effect on yield and resulted in poor yields of products **18a-c**. Formation of the

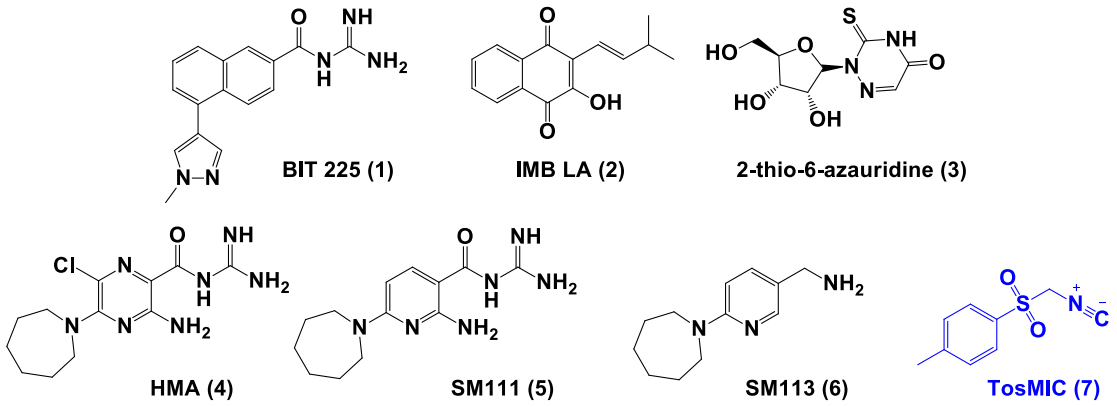

Fig. 2. Structures of HIV-1 Vpu ion channel inhibitors (**1**–**6**) and TosMIC (**7**).

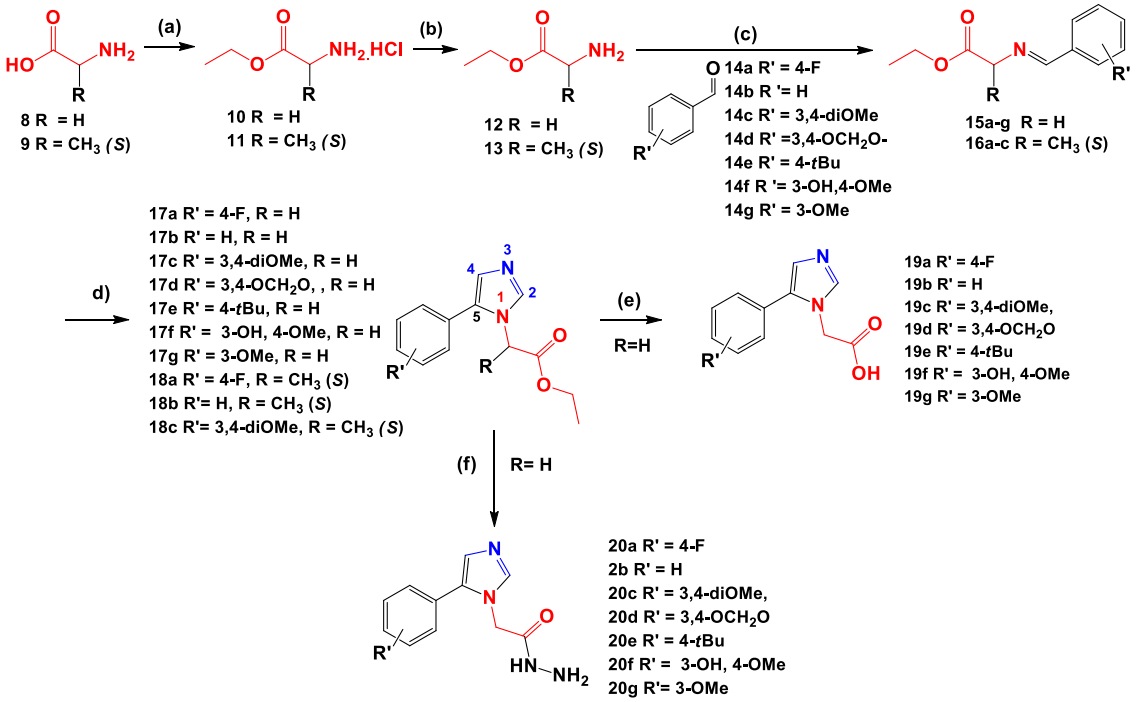

Scheme 1. Synthesis of ethyl 2-(5-aryl-1*H*-imidazol-1-yl)acetates **17** and propionates **18**, 2-(5-aryl-1*H*-imidazol-1-yl)acetic acids **19** and 2-(5-aryl-1*H*-imidazol-1-yl)acetohydrazides **20**:
Reaction conditions: (**a**): $SOCl_2$, EtOH, 0 °C then reflux, 5 h; (**b**) Et_3N $CHCl_3$, r.t. 6 h, then reflux 1 h; (**c**): $MgSO_4$, DCM, r.t. 16 h.; (**d**): TosMIC **7**, DBU, DCM, r.t., 24 h followed by MW: PhMe, 105 °C, 10 min; (**e**) MW: H_2O, 200W, 105 °C, 3 h; (**f**) MW: $NH_2NH_2 \cdot H_2O$, MeOH, 75 °C, 30 min.

imidazole core was confirmed by ^{1}H NMR spectroscopy by the signals corresponding to the 2-methine proton at δ 7.5—8.1 ppm and the 4-methine proton δ 6.8—7.10 ppm (Figs. S1—S20).

The ethyl 2-(5-aryl-1*H*-imidazol-1-yl)acetates **17** were then microwave irradiated in water at a set power of 200 Watts and temperature of 105 °C for 3 h to give a novel set of zwitterionic 2-(5-aryl-1*H*-imidazol-1-yl)acetic acids **19** in good yields (Figs. S21—S34 and Table 1). This zwitterionic form may be attributed to the presence of both the basic imidazole ring and the carboxylic acid, which can tautomerise via internal hydrogen transfer from the carboxylic acid group to the nitrogen of the imidazole ring. (Fig. 3A). Additionally, ethyl 2-(5-aryl-1*H*-imidazol-1-yl)acetates **17** were also subjected to nucleophilic attack by hydrazine monohydrate using a standard microwave method at a set temperature of 75 °C for 30 min to furnish 2-(5-aryl-1*H*-imidazol-1-yl) acetohydrazides **20** as rotamers in excellent yields (Figs. S35—S48 and Table 1). Rotamers arise due to hindered rotation around the amide C—N bond caused by delocalization (Fig. 3B) [60,61].

To confirm that acetohydrazide scaffolds **20** were obtained as rotamers, compound **20e** was chosen to be studied at different temperatures by analyzing the signals around the aromatic region in the ^{1}H NMR spectrum. At 30 °C, the ^{1}H NMR spectrum in DMSO-d_6 of **20e** (Fig. S43) reveals that the relative ratio of the major and minor rotamers is *ca.* 7:1. When the temperature was increased to 70 °C, the signals for the two rotamers began to move closer to each other, but could still be observed (Fig. 4A). Finally, at a temperature of 90 °C, the two signals had coalesced into a single peak. This can be attributed to the fact that at these higher temperatures the rotation barrier between rotamers can be easily overcome, and the interconversion is fast enough when compared to the NMR spectroscopic time-scale.

Table 1
Isolated yields of ethyl 2-(5-aryl-1*H*-imidazol-1-yl)acetates **17** and propionates **18**, 2-(5-aryl-1*H*-imidazol-1-yl) acetic acids **19** and 2-(5-aryl-1*H*-imidazol-1-yl)aceto-hydrazides **20**.

Compounds	R	R′	R"	Yield (%)	Structure
17a	H	4-F	OCH_2CH_3	52	
17b	H	H	OCH_2CH_3	33	
17c	H	3,4-diOMe	OCH_2CH_3	74	
17d	H	3,4-OCH_2O	OCH_2CH_3	45	
17e	H	4-*t*Bu	OCH_2CH_3	35	
17f	H	3-OH,4-OMe	OCH_2CH_3	51	
17g	H	3-OMe	OCH_2CH_3	38	
18a	CH_3 (*S*)	4-F	OCH_2CH_3	11	
18b	CH_3 (*S*)	H	OCH_2CH_3	20	
18c	CH_3 (*S*)	3,4-diOMe	OCH_2CH_3	23	
19a	H	4-F	OH	72	
19b	H	H	OH	68	
19c	H	3,4-diOMe	OH	71	
19d	H	3,4-OCH_2O	OH	68	
19e	H	4-*t*Bu	OH	56	
19f	H	3-OH,4-OMe	OH	58	
19g	H	3-OMe	OH	56	
20a	H	4-F	$NHNH_2$	92	
20b	H	H	$NHNH_2$	90	
20c	H	3,4-diOMe	$NHNH_2$	94	
20d	H	3,4-OCH_2O	$NHNH_2$	90	
20e	H	4-*t*Bu	$NHNH_2$	93	
20f	H	3-OH,4-OMe	$NHNH_2$	94	
20g	H	3-OMe	$NHNH_2$	86	

The existence of rotamers was also observed in the ^{13}C NMR spectrum of compound **20e** (Fig. 4B). Changes in the spectrum around aromatic signals and the carbonyl carbon atom were also detected at different temperatures. At lower temperature, the carbonyl carbon atom of the major rotamer resonates at δ 166.6 ppm, while the minor rotamer emerges at δ 170.9 ppm. The signals of the minor rotamer broaden and then coalesce at temperatures of 70 °C and 90 °C. These results strongly support that extra peaks observed in the NMR spectra of the acetohydrazide scaffolds **20** can be attributed to hindered rotation around the amide C—N bond. A likely explanation for the energetic difference between rotamers **20** and **22**, is that there is the possibility of hydrogen-bond formation between the amide oxygen and the NH_2 group in structure **20**, giving rise to a stable 5-membered ring. This is not a possibility for compound **22** and results in **20** being energetically favoured.

2.2. Biological evaluation

2.2.1. HIV-1 Vpu-BST-2 ELISA assays

A total of 24 novel 2-(5-aryl-1*H*-imidazol-1-yl) scaffolds consisting of acyl, carboxylic acid and acetohydrazide functionalities **17**, **18**, **19** and **20** were initially evaluated for their ability to inhibit the binding of HIV-1 Vpu to the BST-2 protein *via* an enzyme-linked immunosorbent assay (ELISA) [62] at 100 μM concentration and 2-thio-6-azauridine (**3**) was used as a reference (Vpu inhibitor). The percentage inhibition values of the tested compounds were calculated and are listed in Table 2, where seven compounds (**17a**, **17b**, **17c**, **17g**, **18a**, **20f** and **20g**) showed inhibitory activities exceeding a pre-defined cut-off of 50% at 100 μM. Compound **17b** with no substituents on the phenyl ring and no stereogenic centre represented the most potent inhibitory percentage (82%). Compound **20f** with the hydroxyl group and the methoxy group at the *meta*- and *para*-positions of the aryl ring displayed the second highest inhibition percentage of 72%, followed by compound **20g** with the *meta*-methoxyphenyl substituent with 69% inhibition. Compound **18a** (with the *para*-fluorophenyl moiety and a methyl group at the

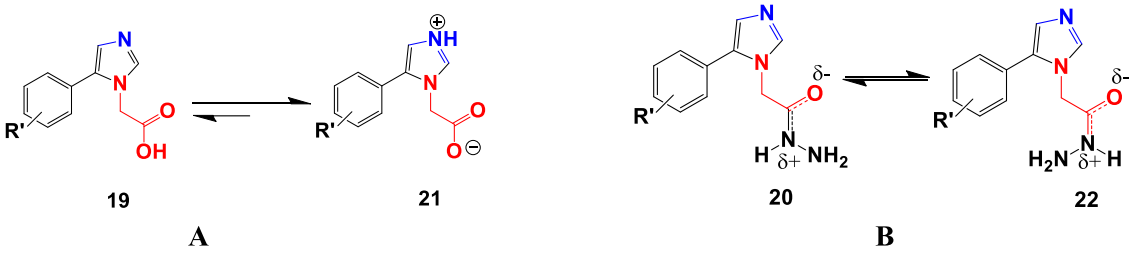

Fig. 3. General representation of **A**: Zwitterionic form of 2-(5-aryl-1*H*-imidazol-1-yl) acetic acids in DMSO-d_6: neutral **19** and ionized form **21**. **B**: Resonance of partial double bond in amide system **20** (major rotamer) and **22** (minor rotamer).

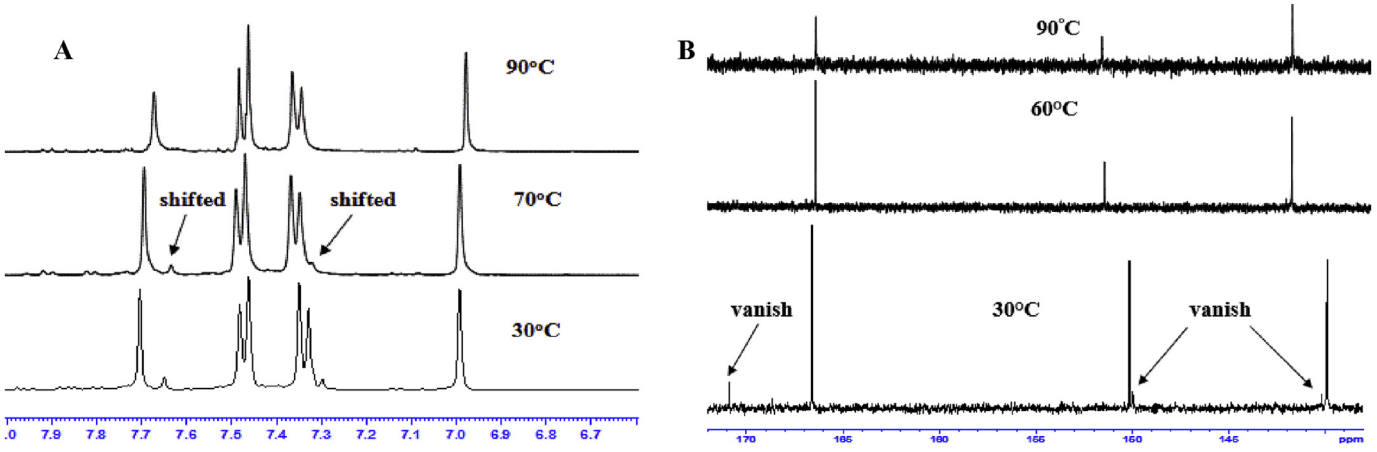

Fig. 4. Effect of temperature on the aromatic signals **A:** in the ^1H NMR spectrum; **B**: in the ^{13}C NMR spectrum of **20e** in DMSO- d_6.

Table 2
ELISA results from screening of ethyl 5-aryl-1*H*-imidazol-1-yl derivatives **17**–**18**, 2-(5-aryl-1*H*-imidazol-1-yl) acetic acids **19** and 2-(5-aryl-1*H*-imidazol-1-yl)acetohydrazides **20**.

Compounds	% inhibition (BST-2 -Vpu ELISA) @ 100 μM
17a	54 ± 0.95
17b	82 ± 1.65
17c	58 ± 2.15
17d	33 ± 2.42
17e	17 ± 1.45
17f	30 ± 2.31
17g	51 ± 3.17
18a	63 ± 1.03
18b	22 ± 1.30
18c	20 ± 0.73
19a	11 ± 4.67
19b	0
19c	25 ± 0.10
19e	9 ± 0.78
19d	2 ± 1.06
19f	0
19g	30 ± 2.31
20a	48 ± 0.14
20b	39 ± 1.33
20c	28 ± 1.57
20d	22 ± 0.68
20e	45 ± 0.57
20f	72 ± 1.42
20g	69 ± 1.40
Reference 3	54 ± 1.68

chiral centre) and compound **17c** (with the methoxy substituents at the *para*- and *meta*-positions and no chiral centre) were ranked fourth and fifth with percentage inhibition activities of 63% and 58%, respectively.

Interestingly, compound **17a**, an analogue of **18a**, with no stereogenic centre ranked sixth with 54% inhibitory activity, which was comparable to the activity found for reference compound **3**. It was not surprising that compound **3** exhibited a modest percentage inhibition as it has been reported to specifically inhibit Vpu-induced BST-2 down-regulation by decreasing Vpu-mediated BST-2 ubiquitination and not necessarily by inhibiting the interaction between the two proteins [32]. Similarly, compound **17g** with the *meta*-methoxyphenyl substituent also exhibited a modest percentage inhibitory activity of 50%. The data further indicated that the acetic acid scaffolds **19a**-**g** exhibited little or no inhibition (0–30%). Overall, these results showed that seven compounds were capable of inhibiting the binding of the HIV-1 Vpu to the host BST-2 protein, which could subsequently lead to prevention of new virion release during HIV-1 replication.

2.2.2. AlphaScreen as a secondary screening assay

To further validate the inhibitory effect of the best potential inhibitors of the HIV-1 Vpu/BST-2 interaction identified, compounds **17a**, **17b**, **17c**, **17g**, **18a**, **20f** and **20g** were further screened using an Amplified Luminescent Proximity Homogeneous Assay (AlphaScreen™ assay) [63] as a secondary test. Prior to the evaluation, the interaction of HIV-1 Vpu with BST-2 protein was established in the AlphaScreen™ assay by using biotinylated recombinant HIV-1 Vpu and a commercially available recombinant GST-tagged BST-2 protein (Abcam). Fixed concentrations of BST-2 (100 nM) bound to anti-GST acceptor beads were treated with the biotinylated HIV-1 Vpu bound to streptavidin donor beads, at different concentrations (0.39–200 nM). The graph shown in Fig. 5A was used to estimate the dissociation constant (K_d) of binding of these two proteins using Origin 6.0 software. The K_d for the binding of HIV-1 Vpu to BST-2 was determined as the concentration of HIV-1 Vpu at which the AlphaScreen signal was reduced by half, and this value was determined to be 4.7 ± 1.62 nM, indicating a strong interaction between these two proteins.

The seven most active compounds from the ELISA assay were then validated in the AlphaScreen™ assay at an initial concentration of 100 μM and their percentage inhibition results are presented in Table 3. From the data obtained, it is evident that all seven compounds were shown to affect the binding of BST-2 to Vpu with percentage inhibition values of greater than the 50% benchmark. Six of the seven compounds (with the exception of compound **20f**), displayed comparable results to those obtained in the ELISA test (Table 3 and Fig. 5B). Inhibition percentages of 83% and 68% were observed for compounds **17b** and **20g**, respectively, while others showed percentage inhibition values (in order) of 64% (**18a**), 61% (**17c**), 60% (**20f**), 56% (**17g**) and 55% (**17a**). Taken together, the ELISA and AlphaScreen results suggest that the seven active hits have the potential to inhibit the binding of HIV-1 Vpu to the BST-2 protein.

Using a dose-response AlphaScreen™ assay, the IC_{50} values of the two compounds exhibiting the highest activities in both assays **(17b** and **20g)** were determined. For the test, compounds with variable concentrations ranging from 200 to 1.56 μM were incubated with the biotinylated HIV-1 Vpu followed by the subsequent addition of BST-2 protein and the IC_{50} determination (Table 3). The data generated from the graph in Fig. 5C showed that compound **17b** displayed a lower IC_{50} value of 11.6 ± 1.1 μM, while compound **20g** exhibited an IC_{50} value of 17.6 ± 0.9 μM.

2.2.3. Cytotoxicity and antiviral assays

The two most active compounds **17b** and **20g** were further assessed for their cytotoxicity effects in the Human T-cell leukaemia (MT-4) mammalian cell line at concentrations ranging from 200 to 1.56 μM. The compounds were screened alongside a control, Auranofin, a compound known to exhibit toxicity against mammalian cells [64]. The results demonstrated that compounds **17b** and **20g** showed marginal cytotoxicity to human cells with CC_{50} values of 184.5 ± 0.8 and 159.5 ± 0.9 μM, respectively (Table 3). The control compound, Auranofin, exhibited a CC_{50} value of 6.5 μM, consistent with the CC_{50} value of 4.5 μM against human HepG-2 human liver cells previously reported [64].

The antiviral effect of these two compounds **17b** and **20g** was evaluated in an *in vitro* phenotypic assay using the MT-4 cell line at concentrations ranging from 200 to 1.56 μM. The compounds were assessed together with FDA-approved inhibitor of HIV-1 replication, Raltegravir, as a positive control, and results are shown in Table 3. Compound **17b** displayed the lowest *in vitro* EC_{50} value of 6.3 ± 0.7 μM, while compound **20g** exhibited an EC_{50} of 157.5 ± 1.2 μM. However, the antiviral activity value (EC_{50}) of **20g** was close to its cytotoxicity value with a selectivity index (SI) of 1, suggesting that the apparent antiviral activity of the compound was in fact the result of its toxicity. On the other hand, compound **17b**, with a SI of 29 represents a good starting point for further modification. Raltegravir produced an EC_{50} of 7.9 ± 0.9 nM, which correlates well with a previously reported EC_{50} value of ≤8 nM [65].

2.3. Aqueous solubility

Poor solubility of an ideal candidate molecule in an *in vitro* assay could lead to poor results, reproducibility and a reduction of compound concentration essential to binding to the target of interest. Compounds **17b** and **20g** and chloramphenicol, used as a control, were assessed to determine their aqueous solubility *in vitro* using the 96-well MultiScreen Solubility Filter plate system from Millipore. The data obtained is recorded in Table 4 and all of these compounds indicated tolerable solubility profiles as classified by the orally absorbed compound guidelines established by Rogge & Taft [66]. Both compounds **17b** and **20g** showed over 100%

Table 3
Biological screening of the most active compounds.

Compounds	Biochemical target assays		Cell-based assays	
	% inhibition (BST-2 Vpu AlphaScreen@100 μM	**IC_{50}[a] (μM)**	**Cytotocity CC_{50}[b] (μM)**	**Antiviral EC_{50}[c] (μM)**
17a	55 ± 0.65			
17b	83 ± 1.66	11.6 ± 1.1	184.5 ± 0.8	6.3 ± 0.7
17c	61 ± 1.23			
17g	56 ± 1.03			
18a	64 ± 1.45			
20f	60 ± 0.98			
20g	68 ± 0.55	17.6 ± 0.9	159.5 ± 0.9	157.5 ± 1.2
BST-2 - Vpu Interaction		*Kd* = 4.7 ± 1.62 nM		
Raltegravir				7.9 ± 0.9 (nM)

[a] IC_{50} -concentration of compound required to inhibit 50% of the specific biological process.
[b] CC_{50} – concentration of compound that causes 50% reduction of cell growth.
[c] EC_{50} - concentration of a drug that gives the half-maximal response.

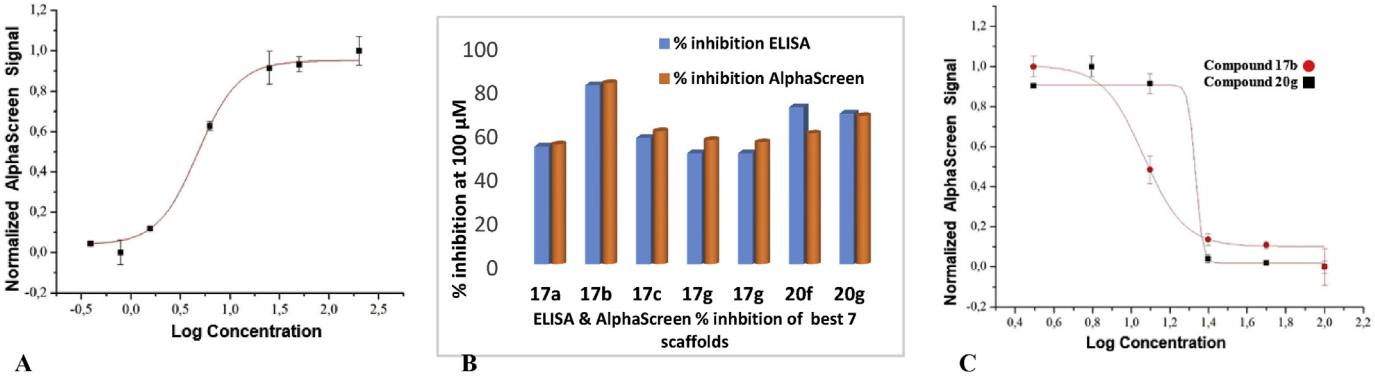

Fig. 5. A: Validation graph of the binding affinity of HIV-1 Vpu to BST-2 in the AlphaScreen™ assay using 100 nM of the GST-tagged BST-2 and Biotinylated HIV-1 Vpu at concentrations ranging from 0.39 to 200 nM. **B**: Comparison of percentage inhibition of the seven active scaffolds in ELISA and AlphaScreen™ assays at 100 μM; **C**: Dose-response curves for Compound **17b** (●) and **20g** (■) generated from AlphaScreen™ assay at different concentrations (200–1.56 μM).

Table 4
The aqueous solubility of the compounds **17b** and **20g** in comparison to chloramphenicol.

Compounds	**Maximum Wavelength nm**	% Dissolution		Solubility (μM)	
		100 μM	200 μM	100 μM	200 μM
17b	250	100	100	≥100	≥200
20g	250	100	100	≥100	≥200
Chloramphenicol	290	100	100	≥100	≥200

Table 5
Analysis of the drug-likeness of the test compounds **17g** and **20g** using Lipinski's rule-of-five.

Compounds	Molecular weight {g/mol} (<500)	H-bond Donors (<5)	H-bond Acceptors (<10)	*Log*P (<5)	Violations
17b	230.26	2	0	2.995	0
20g	246.27	3	2	0.094	0

dissolution at both 100 μM and 200 μM, which is similar to the control compound.

2.4. *In silico prediction of physicochemical properties*

Some physicochemical properties of the two most active candidates **17g** and **20g** were predicted for their compliance with Lipinski's rule-of-five using Biovia Discovery Studio ™ [67,68]. As shown in Table 5, compounds **17g** and **20g** conformed well with Lipinski's rule-of-five. This data further signifies that the identified hits provide a good starting point for further optimization.

3. Conclusion

We have successfully synthesized, *via* TosMIC chemistry, a series of novel ethyl 2-(5-aryl-1*H*-imidazol-1-yl)acyl scaffolds, which were then transformed into two sets of novel 2-(5-aryl-1*H*-imidazol-1-yl) acetic acids and 2-(5-aryl-1H-imidazol-1-yl)acetohydrazides. Assessment of the twenty-four newly synthesized compounds in an HIV-1 Vpu - BST-2 ELISA assay at 100 μM identified seven scaffolds (i.e. **17a**, **17b**, **17c**, **17g**, **18a**, **20f** and **20g**) with high inhibitory activities (>50% inhibition benchmark). Subsequent validation of these hits using an AlphaScreen™ as secondary assay at 100 μM showed that, except for **20f**, the compounds had

comparable percentage inhibitory activities to those found *via* the ELISA assay. The two most active compounds (**17b** and **20g**) were selected for further studies. Cell-based assays indicate that compound **17b** is able to inhibit viral replication without being significantly toxic to the host cells (SI = 29) while the apparent antiviral activity of compound **20g** was attributed to its cytotoxicity (SI = 1). Furthermore, the two most active scaffolds **17b** and **20g** had tolerable solubility profiles and adhered to Lipinski's rule-of-five. The data suggest that the ability of these scaffolds to disrupt the interaction of Vpu and BST-2 could result from preventing binding of virions to the cell surface, thereby limiting virion release. Even though compound **20g** was shown to be toxic, efforts can be made through structure optimization in future to reduce the toxicity while maintaining the desired drug-like properties. Overall, **17g** exhibited high inhibition activities in two biochemical assays, a high antiviral activity, low toxicity and acceptable physicochemical properties, and thus could be considered as a promising candidate for future SAR studies that may guide the rational design and synthesis of possible novel leads for inhibition of the Vpu- BST-2 interaction. To the best of our knowledge, these synthesized compounds are novel and, therefore, have not been reported previously as inhibitors of the binding of HIV-1 Vpu protein to the host BST-2 protein.

4. Experimental section

4.1. General methods and materials

All commercially available reagents were purchased from Sigma-Aldrich. Dry solvents were used from an LC-Tech SP-1 Solvent Purification System stored under argon. Microwave-assisted reactions were performed in a CEM Discover reactor (Dynamic Temperature and Power set). Column chromatography was performed using Merck Silica gel 60 [particle size 0.040–0.063 mm (230–400 mesh)]. TLC was performed on pre-coated Merck silica gel F254 plates and viewed under UV light (254 nm) or following exposure to iodine vapour. NMR spectra were recorded on a 400 MHz Bruker Avance Spectrometer at 298 K equipped with a BBI 5 mm probe. NMR spectra frequency recordings were 400 MHz for ^{1}H and 101 MHz for ^{13}C, using D_2O, $CDCl_3$ or DMSO-d_6 as solvents. Chemical shifts (δ) are cited in parts per million (ppm) and are referenced by the solvent residual peak ($CDCl_3$, δ 7.26 ppm for ^{1}H and δ 77.0 ppm for ^{13}C NMR; DMSO-d_6 δ 2.50 ppm for ^{1}H and δ 39.5 ppm for ^{13}C NMR). High-resolution mass spectra were recorded on an LC-MS system consisting of a Dionex Ultimate 3000 Rapid Separation LC system equipped with a C-18 pre-coated column and coupled to a MicrOTOF QII Bruker mass spectrometer, fitted with an electrospray source operating in positive mode. FTIR spectra were recorded using a Thermo Nicolet 5700 spectrometer and samples were prepared as KBr mixtures. All melting points were obtained using a Stuart SMP10 melting point apparatus and are uncorrected. The compounds 2-thio-6-azauridine, Auranofin, and chloramphenicol used in biological tests were purchased from Sigma-Aldrich and were used as such without further purification. A commercial BST-2 sandwich ELISA kit and a biotin-conjugated anti-BST-2 antibody were purchased from Uscn Life Science.

4.2. Chemistry

4.2.1. Synthesis of ethyl 2-amino hydrochloride salts

4.2.1.1. General synthetic procedure. Thionyl chloride (160 mmol) was added slowly to a mixture containing amino acid (133 mmol) in ethanol (100 ml) at 0 °C. After removal of the ice bath, the mixture was heated at reflux for 5 h. After cooling to room temperature, the ethanol and excess thionyl chloride were removed under reduced pressure. The resultant white solid was combined twice with ethanol and this was again removed under reduced pressure to remove adhering thionyl chloride completely. The product was then recrystallized from ethanol and dried under high vacuum.

*4.2.1.2. Ethyl glycinate hydrochloride **10**.* Physical characteristics: white solid; Yield: 16.71 g, 90%; Mp: 144–147 °C (lit. [69]); ^{1}H NMR (D_2O) 4.36 (2H, q, J = 7.2 Hz, OCH_2CH_3), 3.87 (2H, s, NH_2), 3.61 (2H, s, NCH_2), 1.37 (3H, t, J = 7.1, OCH_2CH_3); ^{13}C NMR (D_2O) 168.5 (*C*=O), 63.4 (OCH_2CH_3), 41.1 (NCH_2), 14.39 (OCH_2CH_3).

*4.2.1.3. L-Ethyl 2-aminopropanoate hydrochloride **11**.* Physical characteristics: white solid; Yield: 20.53 g, 99%; Mp: 76–78 °C (lit. [70]);: ^{1}H NMR (D_2O) 4.10 (2H, q, J = 7.2 Hz, OCH_2CH_3), 3.45 (1H, q, J = 7.2 Hz, $CHCH_3$), 1.62 (2H, s, NH_2), 1.19 (3H, d, J = 7.6 Hz, CH_2CH_3), 1.16 (3H, t, J = 7.6 Hz, OCH_2CH_3); ^{13}C NMR (D_2O) δ 170.2 (C=O), 60.5 (OCH_2CH_3), 49.4 ($CHCH_3$), 19.9 ($CHCH_3$), 14.0 (OCH_2CH_3).

4.2.2. Synthesis of ethyl 2-aminoacylates

4.2.2.1. General synthetic procedure. To a suspension of amino acid ethyl ester hydrochloride (71.6 mmol) in chloroform (15 ml) was added dropwise a solution of triethylamine (71.6 mmol) in chloroform (10 ml) at room temperature. The resulting reaction mixture was stirred at the same temperature for 6 h, followed by heating at reflux for 1 h. The mixture was allowed to cool to room temperature and solvent was removed under reduced pressure to afford a crude material. The product was extracted with diethyl ether (3 × 25 ml) and then filtered. The filtrates were washed with ether (2 × 10 ml). The filtered solution was concentrated *in vacuo* to afford pure ethyl -2-aminoacylates.

*4.2.2.2. Ethyl 2-aminoacetate **12**.* Physical characteristics: yellow oil; Yield: 7.09 g, 96%; ^{1}H NMR ($CDCl_3$) δ 4.14 (2H, q, J = 7.2 Hz, OCH_2CH_3), 3.40 (2H, s, CH_2CO), 1.67 (2H, s, NH_2), 1.23 (3H, t, J = 7.2 Hz, OCH_2CH_3); ^{13}C NMR ($CDCl_3$) δ 174.2 (*C*=O), 60.8 (OCH_2CH_3) 43.9 (CH_2CO), 14.2 (OCH_2CH_3).

*4.2.2.3. L-Alanine ethyl ester **13**.* Physical characteristics: yellow oil; Yield: 8.11 g, 98%: ^{1}H NMR ($CDCl_3$) δ 4.01 (2H, q, J = 7.2 Hz, OCH_2CH_3), 3.43 (1H, q, J = 7.2 Hz, $CHCH_3$), 1.59 (2H, s, NH_2), 1.19 (3H, d, J = 7.4 Hz, $CHCH_3$), 1.13 (3H, t, J = 7.2 Hz, OCH_2CH_3); ^{13}C NMR ($CDCl_3$) δ 176.3 (*C*=O), 60.5 (OCH_2CH_3), 49.8 ($CHCH_3$), 20.4 ($CHCH_3$), 13.9 (OCH_2CH_3).

4.2.3. Preparation of ethyl 2-arylideneamino acyl intermediates

4.2.3.1. General procedure. A solution of free amino acid ethyl ester (27.2 mmol), aryl aldehyde **14** (13.6 mmol) and magnesium sulfate (20.4 mmol) in dry dichloromethane (20 ml) was stirred at room temperature for 16 h. Upon completion, the magnesium sulfate was removed by filtration and washed with DCM. The combined organic layer was concentrated *in vacuo* and the resulting products were kept at 80 °C for 1 h under reduced pressure in a rotary evaporator and finally dried under high vacuum to give pure ethyl 2-arylideneamino acyl intermediates.

*4.2.3.2. (E)-Ethyl 2-(4-fluorobenzylideneamino)acetate **15a**.* Physical characteristics: light yellow oil; Yield: 2.59 g, 91%: ^{1}H NMR ($CDCl_3$) δ 8.20 (1H, s, N=C*H*), 7.71–7.74 (2H, m, Ar*H*), 7.03–7.07 (2H, m, Ar*H*), 4.33 (2H, s, CH_2N), 4.15 (2H, q, J = 7.4 Hz, OCH_2CH_3), 1.23 (3H, t, J = 7.2 Hz, OCH_2CH_3); ^{13}C NMR ($CDCl_3$) δ 170.0 (C=O), 164.5 (d, $^{1}J_{C,F}$ = 247 Hz, *para*-*C*F), 163.8 (N=*C*H), 131.3 (d, $^{4}J_{CF}$ = 3 Hz, 1′-*C*), 115.7 (d, $^{3}J_{CF}$ = 9.0 Hz, *ortho*-*C*), 115.5 (d, ^{2}JCF = 22 Hz, *meta*-*C*), 61.7 (OCH_2CH_3), 60.9 (CH_2N), 14.0 (OCH_2CH_3).

4.2.3.3. (E)-Ethyl 2-(benzylideneamino)acetate ***15b***. Physical characteristics: colourless oil; Yield: 2.49 g, 96%: ^{1}H NMR ($CDCl_3$) δ 8.26 (1H, s, N=C*H*), 7.38–7.76 (5H, m, Ar*H*), 4.37 (2H, s, 2-CH_2), 4.18 (2H, q, J = 7.2 Hz, OCH_2CH$_3$), 1.25- (3H, t, J = 7.2 Hz, OCH$_2$CH_3); ^{13}C NMR ($CDCl_3$) δ 170.0 (*C*=O), 165.8 (N=*C*H), 135.4, 131.7, 128.5, 128.3 (Ar*C*), 61.9 (*C*H$_2$N), 60.9 (OCH_2CH$_3$), 14.1 (OCH$_2$*C*H$_3$).

4.2.3.4. (E)-Ethyl 2-(3,4-dimethoxybenzylideneamino)acetate ***15c***. Physical characteristics: pale yellow oil; Yield: 3.18 g, 93%; ^{1}H NMR ($CDCl_3$) δ 8.15 (1H, s, N=C*H*), 7.42 (1H, s, Ar*H*), 7.13 (1H, dd, J = 6.4 Hz, 1.6 Hz, Ar*H*), 7.13 (1H, d, J = 8.4 Hz, Ar*H*), 4.33 (2H, s, CH_2N), 4.15 (2H, q, J = 7.4 Hz, OCH_2CH$_3$), 3.87 and 3.89 (6H, 2 x s, 2 x ArOCH_3), 1.24 (3H, t, J = 7.4 Hz, OCH$_2$CH_3); ^{13}C NMR ($CDCl_3$) δ 170.2 (*C*=O), 164.8 (N=*C*H), 151.7 and 149.2 (2 x Ar*C*OCH$_3$), 128.8, 123.7, 110.2, 108.7 (Ar*C*), 61.9 (OCH_2CH$_3$), 60.9 (*C*H$_2$N), 55.8 and 55.9 (2 x ArCOCH_3), 14.1 (OCH$_2$*C*H$_3$).

4.2.3.5. (E)-Ethyl 2-((benzo[d][1,3]dioxol-6-yl)methyleneamino)acetate ***15d***. Physical characteristics: pale yellow oil; Yield: 2.92 g, 91%: ^{1}H NMR ($CDCl_3$) δ 8.24 (1H, s, N=C*H*), 7.38 (1H, s, *ArH*), 6.98–7.33 (2H, m, Ar*H*), 4.62 (2H, s, ArOCH_2O-); 4.39 (2H, s, CH_2N), 4.20 (2H, J = 7.2 Hz, OCH_2CH$_3$); 1.27 (3H, q, t, J = 7.2 Hz, OCH$_2$CH_3); ^{13}C NMR ($CDCl_3$) δ 170.0 (*C*=O), 165.3 (N=*C*H), 159.7 and 149.8 (Ar*C*OCH$_2$O), 136.9, 129.4, 121.8, 118.0 (ArC), 101.5 (ArCOCH$_2$O), 61.8 (OCH$_2$CH$_3$), 61.0 (*C*H$_2$N), 14.1 (OCH$_2$*C*H$_3$).

4.2.3.6. (E)-Ethyl 2-(4-tert-butylbenzylideneamino)acetate ***15e***. Physical characteristics: yellow oil; Yield: 2.96 g, 88%; ^{1}H NMR (400 MHz, $CDCl_3$) δ 8.25 (1H, s, N=C*H*), 7.69 (2H, d, J = 8.4 Hz, Ar*H*), 7.42 (2H, q, J = 8.4 Hz, Ar*H*), 4.38 (2H, s, CH_2N), 4.19 (2H, J = 7.4 Hz, OCH_2CH$_3$), 1.32 [9H, s, C(CH_3)$_3$], 1.27 (3H, t, J = 7.0 Hz, OCH$_2$CH_3); ^{13}C NMR (101 MHz; $CDCl_3$) δ 170.2 (*C*=O), 165.2 (N=*C*H), 154.6, 132.9, 128.2, 125.5 (Ar*C*), 62.1 (OCH_2CH$_3$), 60.9 (*C*H$_2$N), 34.9 [Ar*C*(CH$_3$)$_3$], 31.3 [ArC(*C*H$_3$)$_3$], 14.1 (OCH$_2$*C*H$_3$).

4.2.3.7. (E)-Ethyl 2-(3-hydroxy-4-methoxybenzylideneamino)acetate ***15f***. Physical characteristics: orange oil; Yield: 2.78 g, 86%; ^{1}H NMR ($CDCl_3$) δ 8.16 (1H, s, N=C*H*), 7.47 (1H, s, Ar*H*), 7.09 (2H, d, J = 8.4 Hz, Ar*H*), 5.29 (OH), 4.35 (2H, s, CH_2N), 4.20 (2H, q, J = 7.2 Hz, OCH_2CH$_3$), 3.89 (3H, s, ArOCH_3), 1.27 (3H, t, J = 7.2 Hz, OCH$_2$CH_3); ^{13}C NMR ($CDCl_3$) δ 170.0 (*C*=O), 165.3 (N=*C*H), 159.7 (Ar*C*OCH$_3$), 149.8 (Ar*C*OH), 136.9, 118.0, 111.5, 98.0 (Ar*C*), 61.8 (OCH_2CH$_3$), 61.0 (*C*H$_2$N), 55.2 (ArCOCH_3), 14.1 (OCH$_2$*C*H$_3$).

4.2.3.8. (E)-Ethyl 2-(3-methoxybenzylideneamino)acetate ***15g***. Physical characteristics: pale yellow oil; Yield: 2.71 g, 90%; ^{1}H NMR ($CDCl_3$) δ 8.24 (1H, s, N=C*H*), 7.38 (1H, s, Ar*H*), 6.98–7.33 (3H, m, Ar*H*), 4.39 (2H, s, CH_2N), 4.20 (2H, q, J = 7.2 Hz, OCH_2CH$_3$), 3.83 (3H, s, ArOCH_3), 1.27 (3H, t, J = 7.2 Hz, OCH$_2$CH_3); ^{13}C NMR ($CDCl_3$) δ 170.0 (*C*=O), 165.3 (N=*C*H), 159.7 (Ar*C*OCH$_3$), 136.9, 129.4, 121.8, 118.0, 111.5 (Ar*C*), 61.8 (OCH_2CH$_3$), 61.0 (*C*H$_2$N), 55.2 (ArCOCH_3), 14.1 (OCH$_2$*C*H$_3$).

4.2.3.9. (S, E)-Ethyl 2-(4-fluorobenzylideneamino)propanoate ***16a***. Physical characteristics: pale yellow oil; Yield: 2.77 g, 91%; ^{1}H NMR ($CDCl_3$) δ 8.29 (1H, s, N=C*H*), 7.74–7.76 (2H, m, Ar*H*), 7.38 (2H, t, J = 8.4 Hz, Ar*H*), 4.11–4.21 (3H, m, C*H*CH$_3$ and OCH_2CH$_3$), 1.50 (3H, q, J = 7.2 Hz, CHCH_3), 1.23 (3H, t, J = 7.2 Hz, OCH$_2$CH_3); ^{13}C NMR ($CDCl_3$) δ 170.0 (*C*=O), 164.4 (d, $^1J_{C,F}$ = 247 Hz, *para*-*C*F), 163.8 (N=*C*H), 131.4 (d, $^4J_{CF}$ = 3 Hz, 1′-*C*), 126.4 (d, $^3J_{CF}$ = 9 Hz, *ortho*-*C*), 115.5 (d, $^2J_{CF}$ = 22 Hz, *meta*-*C*), 66.8 (*C*HCH$_3$), 61.7 (OCH$_2$CH$_3$), 18.3 (CH*C*H$_3$), 14.0 (OCH$_2$*C*H$_3$).

4.2.3.10. (S, E)-Ethyl 2-(benzylideneamino)propanoate ***16b***. Physical characteristics: light yellow oil; Yield: 2.01 g, 72%; ^{1}H NMR ($CDCl_3$) δ 8.39 (1H, s, N=C*H*), 7.40–7.55 (5H, m, Ar*H*), 4.11–4.25 (3H, m, C*H*CH$_3$ and OCH_2CH$_3$), 1.28 (3H, q, J = 7.4 Hz, CHCH_3), 1.18 (3H, t, J = 7.0 Hz, OCH$_2$CH_3); ^{13}C NMR ($CDCl_3$) δ 172.8 (*C*=O), 162.7 (N=*C*H), 135.9, 131.6, 128.9, 128.6 (Ar*C*), 68.4 (*C*HCH$_3$), 61.0 (OCH_2CH$_3$), 19.3 (CH*C*H$_3$), 14.1 (OCH$_2$*C*H$_3$).

4.2.3.11. (S, E)-Ethyl 2-(3,4-dimethoxybenzylideneamino)propanoate ***16c***. Physical characteristics: pale yellow oil; Yield: 3.00 g, 83%; ^{1}H NMR ($CDCl_3$) δ 8.17 (1H, s, N=C*H*), 7.41 (1H, s, Ar*H*), 7.14 (1H, d, J = 8.4 Hz, Ar*H*), 6.82 (1H, d, J = 8.4 Hz, Ar*H*), 4.05–4.18 (3H, m, C*H*CH$_3$ and OCH_2CH$_3$), 3.86 and 3.89 (6H, 2 x s, 2 x ArOCH_3), 1.46 (3H, J = 7.4 Hz, CHCH_3), 1.21 (3H, t, J = 7.2 Hz, OCH$_2$CH_3); ^{13}C NMR ($CDCl_3$) δ 172.6 (*C*=O), 162.2 (N=*C*H), 151.5 and 149.1 (2 x Ar*C*OCH$_3$), 128.9, 123.5, 110.1, 108.8 (Ar*C*), 67.7 (*C*HCH$_3$), 60.8 (OCH_2CH$_3$), 55.9 and 55.8 (2 x ArCOCH_3), 19.3 (CH*C*H$_3$), 14.0 (OCH$_2$*C*H$_3$).

4.2.4. Synthesis of ethyl 2-(5-aryl-1H-imidazol-1-yl)acyl derivatives

4.2.4.1. Synthetic procedure. To a stirred solution of ethyl 2-(arylideneamino)acylate (2.04 mmol), TosMIC (2.04 mmol) and DCM (8 ml), a solution of DBU (2.04 mmol) in DCM (2 ml) was added dropwise at room temperature. Thereafter, the resulting mixture was stirred for 24 h. After consumption of TosMIC, the solvent was evaporated and the brown oily crude material obtained was re-dissolved in toluene (10 ml) and transferred into a 35 ml microwave vessel equipped with a magnetic stirrer bar and capped. The resulting solution was microwave irradiated at a set temperature of 115 °C for 10 min. After the solution cooled down, the solvent was evaporated to afford a dark brown oily crude material, which was purified by flash column chromatography [first elution (2:1) hexane: ethyl acetate, followed by 1% MeOH in ethyl acetate] to afford the pure product.

4.2.4.2. Ethyl 2-[5-(4-fluorophenyl)-1H-imidazol-1-yl]acetate ***17a***. Physical characteristics: brown oil; Yield: 263 mg, 52%; ^{1}H NMR ($CDCl_3$) δ 7.55 (1H, s, 2-C*H*), 7.25–7.28 (2H, m, Ar*H*), 7.06–7.10 (2H, t, J = 8.6 Hz, Ar*H*), 7.02 (1H, s, 4-C*H*), 4.60 (2H, s, NCH_2), 4.12 (2H, q, J = 7.2 Hz, OCH_2CH$_3$), 1.17 (3H, t, J = 7.2 Hz, OCH$_2$CH_3); ^{13}C NMR ($CDCl_3$) δ 167.6 (*C*=O), 163.7 (d, $^1J_{C,F}$ = 249 Hz, *para*-*C*F), 138.9 (2-*C*), 132.3 (5-*C*), 130.8 (d, $^3J_{C,F}$ = 8 Hz, *ortho*-*C*), 127.9 (4-*C*), 125.1 (d, $^4J_{C,F}$ = 3 Hz, 1′-*C*), 115.7 (d, $^2J_{C,F}$ = 22.1 Hz, *meta*-*C*), 62.0 (OCH_2CH$_3$), 46.2 (NCH_2), 13.9 (OCH$_2$CH_3); FTIR νmax/cm-1 (KBr): 3104, 3026, 1747, 1568, 1496, 1380, 1478, 1278, 1163, 854, 824, 698, 694, 543; HRMS (ESI-TOF) *m*/*z*: $[M+H]^+$ Calcd for $C_{13}H_{14}FN_2O_2$ 249.1034, found 249.1037.

4.2.4.3. Ethyl 2-[(5-phenyl)-1H-imidazol-1-yl]acetate ***17b***. Physical characteristics: pale yellow solid; Yield: 155 mg, 33%; Mp: 144–147 °C; ^{1}H NMR ($CDCl_3$) δ 7.58 (1H, s, 2-C*H*), 7.29–7.41 (5H, m, Ar*H*), 7.08 (1H, s, 4-C*H*), 4.66 (2H, s, NCH_2), 4.14 (2H, q, J = 7.2 Hz, OCH_2CH$_3$), 1.18 (3H, t, J = 7.2 Hz, OCH$_2$CH_3); ^{13}C NMR ($CDCl_3$) δ 167.7 (*C*=O), 139.0 (2-*C*), 133.4 (5-*C*), 129.1, 128.9, 128.8, 128.3 (Ar*C*), 127.8 (4-*C*), 62.0 (OCH_2CH$_3$), 46.4 (NCH_2), 13.9 (OCH$_2$CH_3); FTIR νmax/cm-1 (KBr): 3122, 2936, 2954, 1736, 1602, 1484, 1444, 1376, 1321, 1216, 1160, 1118, 1080, 978, 852, 824, 768, 700, 660; HRMS (ESI-TOF) *m*/*z*: $[M+H]^+$ Calcd for $C_{13}H_{15}N_2O_2$ 231.1128, found 231.1126.

4.2.4.4. Ethyl 2-[5-(3,4-dimethoxyphenyl)-1H-imidazol-1-yl]acetate ***17c***. Physical characteristics: yellow solid; Yield: 438 mg, 74%; Mp: 67–70 °C; ^{1}H NMR ($CDCl_3$) δ 7.56 (1H, s, 2-C*H*), 7.01 (1H, s, 4-C*H*), 6.81–6.88 (3H, m, Ar*H*), 4.61 (2H, s, NCH_2), 4.13 (2H, q, J = 7.2 Hz, OCH_2CH$_3$) 3.83 and 3.87 (6H, 2 x s, 2 x ArOCH_3), 1.18 (3H, t, J = 7.2 Hz, OCH$_2$CH$_3$); ^{13}C NMR (CDC_{l3}) δ 167.8 (*C*=O), 149.2 and 148.9 (2 x Ar*C*OCH$_3$), 138.5 (2-*C*), 133.3 (5-*C*), 127.3, 121.6, (Ar*C*),

121.5 (4-*C*), 112.3, 111.2 (Ar*C*), 61.9 (OCH_2CH_3), 55.81 and 55.78 (2 x $ArCOCH_3$), 46.3 (NCH_2), 13.9 (OCH_2CH_3); FTIR νmax/cm-1 (KBr): 2955, 2930, 1748, 1617, 1566, 1503, 1435, 1356, 1217, 1143, 1039, 759, 665, 513; HRMS (ESI-TOF) *m/z*: $[M+H]^+$ Calcd for $C_{15}H_{21}N_2O_4$ 291.1339, found 291.1332.

4.2.4.5. Ethyl 2-(5-(benzo[d][1,3]dioxol-6-yl)-1H-imidazol-1-yl)acetate ***17d***. Physical characteristics: pale yellow solid; Yield: 252 mg, 45%; Mp: 83–86 °C; ^{1}H NMR ($CDCl_3$) δ 7.52 (1H, s, 2-C*H*), 6.97 (1H, s, 4-C*H*), 6.79 (1H, d, *J* = 7.4 Hz, Ar*H*), 6.71–6.72 (2H, overlapping singlet and doublet, Ar*H*), 5.95 (2H, s, $ArOCH_2O$), 4.60 (2H, s, NCH_2), 4.13 (2H, q, *J* = 7.2 Hz, OCH_2CH_3), 1.18 (3H, t, *J* = 7.2 Hz, OCH_2CH_3); ^{13}C NMR ($CDCl_3$) δ 167.7 (*C*=O), 147.8 and 148.7 (2 x $ArCOCH_2O$), 138.6 (2-*C*), 133.0 (5-*C*), 127.4, (Ar*C*), 122.8 (4-*C*), 122.5, 109.4, 108.5 (Ar*C*), 101.2 ($ArCOCH_2O$), 61.9 (OCH_2CH_3), 46.2 (NCH_2), 13.9 (OCH_2CH_3); FTIR νmax/cm-1 (KBr): 3097, 2986, 2908, 2782, 1741, 1504, 1479, 1336, 1243, 1213, 1104, 1041, 921, 887, 813; HRMS (ESI-TOF) *m/z*: $[M+H]^+$ Calcd for $C_{13}H_{13}N_2O_4$ 261.1183, found 261.1186.

4.2.4.6. Ethyl 2-(5-(4-tert-butylphenyl)-1H-imidazol-1-yl)acetate ***17e***. Physical characteristics: brown oil; Yield: 204 mg, 35%; ^{1}H NMR ($CDCl_3$) δ 7.64 (1H, s, 2-C*H*), 7.45 (2H, d, *J* = 8.4 Hz, Ar*H*), 7.28 (2H, d, *J* = 8.4 Hz, Ar*H*), 7.10 (1H,s, 4-C*H*), 4.70 (2H, s, NCH_2), 4.19 (2H, q, *J* = 7.2 Hz, OCH_2CH_3), 1.37 [9H, s, $C(CH_3)_3$], 1.21 (3H, t, *J* = 7.2 Hz, OCH_2CH_3); ^{13}C NMR ($CDCl_3$) δ 167.8 (*C*=O), 151.5 [Ar*C*$(CH_3)_3$], 138.8 (2-*C*), 133.4, 128.6, 127.5, 126.1, 125.7 (Ar*C*), 62.0 (OCH_2CH_3), 46.4 (NCH_2), 34.6 [Ar*C*$(CH_3)_3$], 31.2 [ArC$(CH_3)_3$], 14.0 (OCH_2CH_3); FTIR νmax/cm-1 (KBr): 2966, 2904, 2870, 1755, 1480, 1363, 1265, 1219, 1113, 1011, 913, 840, 656, 565; HRMS (ESI-TOF) *m/z*: $[M+H]^+$ Calcd for $C_{17}H_{23}N_2O_2$ 287.1754, found 287.1764.

4.2.4.7. Ethyl 2-(5-(3-hydroxy-4-methoxyphenyl)-1H-imidazol-1-yl) acetate ***17f***. Physical characteristics: yellow solid; Yield: 288 mg, 51%; Mp: 137–140 °C; ^{1}H NMR ($CDCl_3$) δ 7.76 (1H, s, 2-C*H*), 7.05 (1H, s, 4-C*H*),6.95 (1H, d, *J* = 8.4 Hz, Ar*H*), 6.76–6.81 (2H, m, Ar*H*), 5.24 (1H, br s, ArO*H*), 4.67 (2H, s, NCH_2), 4.16 (2H, q, *J* = 7.2 Hz, OCH_2CH_3), 3.87 (3H, s, $ArOCH_3$), 1.21 (3H, t, *J* = 7.2 Hz, OCH_2CH_3); ^{13}C NMR ($CDCl_3$) δ 167.8 (*C*=O), 147.0 and 146.7 (Ar*C*OCH_3 and Ar*C*OH), 138.2 (NCH_2), 133.8 (5-*C*), 126.0, 122.5 (Ar*C*), 120.1 (4-*C*), 115.0, 112.2 (Ar*C*), 62.2 (OCH_2CH_3), 56.0 ($ArCOCH_3$), 46.5 (NCH_2), 14.1 (OCH_2CH_3); FTIR νmax/cm-1 (KBr): 2974, 2929, 2608, 1748, 1596, 1552, 1501, 1494, 1474, 1334, 1213, 1112, 1026, 956, 813, 616; HRMS (ESI-TOF) *m/z*: $[M+H]^+$ Calcd for $C_{14}H_{17}N_2O_4$ 277.1183, found 277.1184.

4.2.4.8. Ethyl 2-[5-(3-methoxyphenyl)-1H-imidazol-1-yl]acetate ***17g***. Physical characteristics: brownish yellow oil; Yield: 202 mg, 38%; ^{1}H NMR ($CDCl_3$) δ 7.57 (1H, s, 2-C*H*), 7.29–7.33 (1H, m, Ar*H*), 7.08 (1H, s, 4-C*H*), 6.84–6.92 (3H, m, Ar*H*), 4.66 (2H, s, NCH_2), 4.15 (2H, q, *J* = 7.2 Hz, OCH_2CH_3), 3.79 (3H, s, $ArOCH_3$), 1.19 (3H, t, *J* = 7.2 Hz, OCH_2CH_3); ^{13}C NMR ($CDCl_3$) δ 167.7 (*C*=O), 159.8 (Ar*C*OCH_3), 139.0 (2-*C*), 133.2 (5-*C*), 130.3, 129.8, 127.8 (Ar*C*), 121.01 (4-*C*), 114.3, 113.9 (Ar*C*), 62.0 (OCH_2CH_3), 46.4 (NCH_2), 13.9 (OCH_2CH_3); FTIR νmax/cm-1 (KBr): 3126, 2887, 1745, 1604, 1591, 1536, 1453, 1425, 1379, 1326, 1292, 1225, 1027, 928, 800, 699, 516; HRMS (ESI-TOF) *m/z*: $[M+H]^+$ Calcd for $C_{14}H_{17}N_2O_3$ 261.1234, found 261.1232.

4.2.4.9. (S)-Ethyl 2-(5-(4-fluorophenyl)-1H-imidazol-1-yl)propanoate ***18a***. Physical characteristics: pale yellow oil; Yield: 59 mg, 11%; ^{1}H NMR ($CDCl_3$) δ 7.52 (1H, s, 2-C*H*), 7.20–7.24 (2H, m, Ar*H*), 7.02 (2H, t, *J* = 8.8 Hz, Ar*H*), 6.97 (1H, s, 4-C*H*), 4.56 (2H, s, NCH_2), 4.81 (1H, q, *J* = 7.2 Hz, $CHCH_3$), 4.17–4.25 (2H, q, *J* = 7 Hz, OCH_2CH_3), 1.65–1.72 (3H, d, *J* = 8 Hz, $CHCH_3$), 1.14 (3H, t, *J* = 7.2 Hz, OCH_2CH_3); ^{13C} NMR ($CDCl_3$) δ 167.4 (*C*=O), 162.5 (d, $^1J_{C,F}$ = 249 Hz, *para*-*C*F), 138.7 (2-*C*), 132.1 (5-*C*), 130.6 (d, $^3J_{C,F}$ = 9 Hz, *ortho*-*C*), 127.7 (4-C), 124.9 (d, $^4J_{C,F}$ = 3.0 Hz, 1′-*C*), 115.6 (d, $^2J_{C,F}$ = 21 Hz, *meta*-*C*), 61.8 (OCH_2CH_3), 46.0 ($CHCH_3$), 20.5 ($CHCH_3$), 14.1 (OCH_2CH_3); FTIR νmax/cm-1 (KBr): 2955, 2930, 1748, 1617, 1566, 1503, 1435, 1356, 1217, 1143, 1039, 759, 665, 513; HRMS (ESI-TOF) *m/z*: $[M+H]^+$ Calcd for $C_{14}H_{16}FN_2O_2$ 263.1173, found 263.1190.

4.2.4.10. (S)-Ethyl 2-(5-phenyl-1H-imidazol-1-yl)propanoate ***18b***. Physical characteristics: yellow solid; Yield: 100 mg, 20%; ^{1}H NMR ($CDCl_3$) δ 7.76 (1H, s, 2-C*H*), 7.37–7.41 (3H, m, Ar*H*), 7.27–7.29 (2H, m, Ar*H*), 7.03 (1H, s, 4-C*H*), 4.80 (1H, q, *J* = 8.4 Hz, $CHCH_3$), 4.12 (2H, q, *J* = 7.2 Hz, OCH_2CH_3), 1.70 (3H, d, *J* = 7.2 Hz, $CHCH_3$), 1.17 (3H, t, *J* = 7.2 Hz, OCH_2CH_3); ^{13}C NMR ($CDCl_3$) δ 170.3 (*C*=O), 136.0 (2-*C*), 133.1 (5-*C*), 129.3, 129.2, 128.7, 128.3, 127.2 (Ar*C*), 61.9 (OCH_2CH_3), 52.9 ($CHCH_3$), 18.8 ($CHCH_3$), 13.9 (OCH_2CH_3); HRMS (ESI-TOF) *m/z*: $[M+H]^+$ Calcd for $C_{14}H_{17}N_2O_2$ 245.1258; found 245.1279.

4.2.4.11. (S)-Ethyl 2-(5-(3,4-dimethoxyphenyl)-1H-imidazol-1-yl) propanoate ***18c***. Physical characteristics: yellow solid; Yield: 143 mg, 23%; ^{1}H NMR ($CDCl_3$) δ 7.69 (1H, s, 2-C*H*), 6.96 (1H, s, 4-C*H*), 6.78–6.88 (3H, m, Ar*H*), 4.78 (1H, q, *J* = 8.4 Hz, $CHCH_3$), 4.10 (2H, q, *J* = 7.2 Hz, OCH_2CH_3), 3.82 and 3.86 (6H, 2 x s, $ArOCH_3$), 1.66 (3H, d, *J* = 7.2 Hz, $CHCH_3$), 1.16–1.20 (3H, t, *J* = 7.2 Hz, OCH_2CH_3); ^{13}C NMR ($CDCl_3$) δ 167.4 (*C*=O), 149.15 and 148.9 (2 x Ar*C*OCH_3), 135.7 (2-*C*), 130.7 (5-*C*), 127.5, 127.7, 127.6, 112.6, 111.2 (Ar*C*), 61.8 (OCH_2CH_3), 55.8 and 55.7 (2 x Ar*C*OCH_3), 52.8 ($CHCH_3$), 18.8 ($CHCH_3$), 13.9 (OCH_2CH_3); FTIR νmax/cm-1 (KBr): 3635, 2954, 2896, 2783, 1750, 1668, 1479, 1440, 1378, 1306, 1225, 1108, 1038, 933, 880, 815, 726, 668, 579; HRMS (ESI-TOF) *m/z*: $[M+H]^+$ Calcd for $C_{16}H_{21}N_2O_4$ 305.1476, found 305.1503.

4.2.5. Synthesis of 2-(5-aryl)-1H-imidazol-1-yl)acetic acid derivatives

4.2.5.1. Synthetic procedure. In a 35 ml microwave vessel equipped with a magnetic stirrer bar, was added ethyl 2-(5-aryl-1*H*-imidazol-1-yl)acetate **17** (0.96 mmol) and water (25 ml). The cap was replaced and the resulting mixture was microwave irradiated at a set power of 200 W and a temperature of 105 °C for 3 h. After completion of the reaction, the mixture was transferred into a separating funnel, water (5 ml) was added, followed by washing with ethyl acetate (3 × 10 ml). The water layer was evaporated *in vacuo* and dried under high vacuum to afford the desired pure 2-(5-aryl)-1*H*-imidazol-1-yl)acetic acids.

4.2.5.2. 2-[5-(4-Flurorophenyl)-1H-imidazol-1-yl]acetic acid ***19a***. Physical characteristics: pale yellow solid; Yield: 152 mg, 72%; Mp: 189–192 °C; ^{1}H NMR (DMSO-d_6) δ 7.85 (1H, s, 2-C*H*), 7.41–7.45 (2H, m, Ar*H*), 7.06–7.31 (2H, m, Ar*H*), 7.07 (1H, s, 4-C*H*), 4.84 (2H, s, NCH_2);^{13}C NMR (DMSO-d_6) δ 169.7 (*C*=O), 160.7 (d, $^1J_{C,F}$ = 246 Hz, *para*-*C*F), 139.8 (2-*C*), 131.8 (5-*C*), 130.3 (d, $^3J_{C,F}$ = 8 Hz, *ortho*-*C*), 126.6 (4-*C*), 125.8 (d, $^4J_{C,F}$ = 3 Hz, 1′-*C*), 115.7 (d, $^2J_{C,F}$ = 22 Hz, *meta*-*C*), 46.5 (NCH_2); FTIR νmax/cm-1 (KBr): 3105, 3032, 2434, 1645, 1540,1496, 1380, 1290, 1226, 1165, 1110, 544, 823, 767, 697, 693, 544; HRMS (ESI-TOF) *m/z*: $[M+H]^+$ Calcd for $C_{11}H_{10}FN_2O_2^+$ 221.0721, found 221.0720.

4.2.5.3. 2-(5-Phenyl-1H-imidazol-1-yl)acetic acid ***19b***. Physical characteristics: pale yellow solid; Yield: 132 mg, 68%; Mp: 175–178 °C; ^{1}H NMR ($CDCl_3$) δ 10.1 (1H, s, O*H*), 8.62 (1H, s, 2-C*H*), 7.30 (5H, m, Ar*H*), 7.07 (1H, s, 4-C*H*), 4.61 (2H, s, NCH_2); ^{13}C NMR ($CDCl_3$) δ 170.9 (*C*=O), 137.5 (2-*C*), 134.3 (5-*C*), 129.4, 129.2 (Ar*C*), 129.0 (4-*C*), 126.5, 119.0 (Ar*C*), 49.2 ((NCH_2); FTIR νmax/cm-1 (KBr): 3139, 2957, 2900, 2861, 2517, 1730, 1691, 1626, 1378, 1270, 1113, 766, 687; HRMS (ESI-TOF) *m/z*: $[M+H]^+$ Calcd for $C_{11}H_{11}N_2O_2$ 203.0815; found 203.0807.

4.2.5.4. 2-[5-(3,4-Dimethoxyphenyl)-1H-imidazol-1-yl]acetic acid ***19c***. Physical characteristics: yellow solid; Yield: 179 mg, 71%; Mp: 124–127 °C; ^{1}H NMR (DMSO-d_6) δ 7.77 (1H, s, 2-C*H*), 6.88–67.02 (4H, overlapping signals, m, Ar*H* and 4-C*H*), 4.74 (2H, s, NCH_2), 3.77 and 3.74 (6H, 2 x s, 2 x ArOCH_3); ^{13}C NMR (DMSO-d_6) δ 170.3 (*C*=O), 148.7 and 148.7 (2 x Ar*C*OCH$_3$), 139.4 (2-*C*), 132.8 (5-*C*), 125.9, 127.8 (Ar*C*), 120.7 (4-*C*), 112.0, 111.9 (Ar*C*), 55.5 and 55.4 (2 x ArCOCH$_3$), 46.9 (NCH$_2$); FTIR νmax/cm-1 (KBr): 3126, 3050, 2970, 2841, 2604, 1612, 1512, 1471, 1447, 1380, 1324, 1256, 1224, 1181, 1146, 1021, 826, 806, 695, 676; HRMS (ESI-TOF) *m*/*z*: [M+H]$^+$ Calcd for $C_{13}H_{15}N_2O_4$ 263.1040, Found 263.1017.

4.2.5.5. 2-(5-(Benzo[d][1,3]dioxol-6-yl)-1H-imidazol-1-yl)acetic acid ***19d***. Physical characteristics: yellow solid; Yield: 161 mg, 68%; Mp: 233–236 °C; ^{1}H NMR (DMSO-d_6) δ 7.79(1H, s, 2-C*H*),6.82–6.99 (4H, overlapping signals, m, Ar*H* and 4-C*H*), 6.05 (2H, s, ArOCH_2O), 4.77 (2H, s, NCH_2); ^{13}C NMR (DMSO-d_6) δ 170.0 (*C*=O), 147.6 and 147.1 (Ar*C*OCH$_2$O), 139.4 (2-*C*), 132.6 (5-*C*), 126.2, 123.0, 122.1, 108.7 (Ar*C*), 101.4 (ArCOCH$_2$O), 46.7 (NCH$_2$); FTIR νmax/cm-1 (KBr): 3435, 3152, 3096, 2500, 1652, 1604, 1504, 1474, 1388, 1313, 1257, 1226, 1035, 882, 691; HRMS (ESI-TOF) *m*/*z*: [M+H]$^+$ Calcd for $C_{12}H_{11}N_2O_4$ 247.0713, found 247.0702.

4.2.5.6. 2-(5-(4-tert-Butylphenyl)-1H-imidazol-1-yl)acetic acid ***19e***. Physical characteristics: yellow solid; Yield: 333 mg, 56%; Mp: 170–173 °C; ^{1}H NMR (DMSO-d_6) δ 7.82 (1H, s, 2-C*H*), 7.45 (2H, d, *J* = 7.6 Hz, Ar*H*), 7.30 (2H, d, *J* = 7.6 Hz, Ar*H*), 7.04 (1H, s, 4-C*H*), 4.81 (2H, s, NCH_2), 1.29 [9H, s, C(CH_3)$_3$]; ^{13}C NMR (DMSO-d_6) δ 169.9 (*C*=O), 150.4 [Ar*C*C(CH$_3$)$_3$], 139.7 (2-*C*), 132.7, 127.7, 126.5, 126.3, 125.7 (Ar*C* and 4-*C*), 46.7 (N*C*H$_2$), 34.4 [ArC*C*(CH$_3$)$_3$], 31.1 [ArCC(*C*H$_3$)$_3$]; FTIR νmax/cm-1 (KBr): 3132, 3035, 2961, 2905, 2868, 2509, 1722, 1678, 1625, 1463, 1378, 1335, 1269, 1233, 1112, 1035, 1010, 841, 677; HRMS (ESI-TOF) *m*/*z*: [M+H]$^+$ Calcd for $C_{15}H_{19}N_2O_2$ 259.1441, Found 259.1440.

4.2.5.7. 2-(5-(3-Hydroxy-4-methoxyphenyl)-1H-imidazol-1-yl)acetic acid ***19f***. Physical characteristics: yellow solid; Yield: 138 mg, 58%; Mp: 211–214 °C; ^{1}H (DMSO-d_6) δ 7.85 (1H, s, 2-C*H*), 7.00 (1H, s, 4-C*H*), 6.89 (1H, s, 4-C*H*), 6.82 (1H, d, *J* = 8.0 Hz, Ar*H*), 6.75 (2H, d, *J* = 8.0, Ar*H*), 5.57 (1H, br, ArO*H*), 4.75 (2H, s, NCH_2), 3.76 (3H, s, ArOCH_3); ^{13}C NMR (NMR (DMSO-d_6) δ 166.7 (*C*=O), 147.6 and 146.5 (Ar*C*OCH$_3$ and Ar*C*OH), 139.3 (2-*C*), 133.1 (5-*C*), 126.2 (Ar*C*), 121.2 (4-*C*), 120.4, 115.7, 112.4 (Ar*C*), 55.6 (ArCOCH_3), 45.7 (NCH_2); FTIR νmax/cm-1 (KBr): 2973, 2930, 2600, 1748, 1604, 1552, 1514, 1358, 1312, 1280, 1214, 1139, 1109, 1026, 865, 822; HRMS (ESI-TOF) *m*/*z*: [M+H]$^+$ Calcd for $C_{12}H_{13}N_2O_4$ 249.2421, found 249.2438.

4.2.5.8. 2-[5-(3-Methoxyphenyl)-1H-imidazol-1-yl]acetic acid ***19g***. Physical characteristics: yellow solid; Yield: 125 mg, 56%; ^{1}H NMR (DMSO-d_6) δ 7.83 (1H, s, 2-C*H*), 7.33–7.37 (1H, m, Ar*H*), 7.09 (1H, s, 4-C*H*), 6.93–6.96 (3H, m, Ar*H*), 4.81 (2H, s, NCH_2), 3.76 (3H, s, ArOCH_3);^{13}C NMR (DMSO-d_6) δ 170.1 (*C*=O), 159.5 (Ar*C*OCH$_3$), 140.0 (2-*C*), 132.7 (5-*C*), 130.7, 130.0, 126.6 (Ar*C*), 120.3 (4-*C*), 113.6, 113.4 (Ar*C*), 55.1 (ArCOCH_3), 46.9 (NCH_2); FTIR νmax/cm-1 (KBr): 3126, 2946, 2450, 1696, 1609, 1578, 1487, 1394, 1300, 1207, 1168, 1028, 854, 777, 693; HRMS (ESI-TOF) *m*/*z*: [M+H]$^+$ Calcd for $C_{12}H_{13}N_2O_3$ 233.0921, found 233.0922.

4.2.6. Synthesis of 2-(5-aryl-1H-imidazol-1-yl)acetohydrazide

4.2.6.1. General synthetic procedure. Ethyl 2-(5-aryl-1*H*-imidazol-1-yl)acylate (0.90 mmol) and hydrazine monohydrate (2.70 mmol) and MeOH (5 ml) were placed in a 10 ml microwave vessel equipped with a magnetic stirrer bar. The cap was then fitted and the resulting mixture was microwave irradiated at a set temperature of 75 °C for 30 min. After completion of the reaction, the solvent was removed and DCM was added to generate a precipitate which was then filtered and dried under high vacuum to afford pure 2-(5-aryl-1*H*-imidazol-1-yl)acetohydrazides.

(**NB**: ^{1}H and ^{13}C NMR spectra reported below are for major rotamer only).

4.2.6.2. 2-[5-(4-Fluorophenyl)-1H-imidazol-1-yl]acetohydrazide ***20a***. Physical characteristics: white solid; Yields: 194 mg, 92%; Mp: 178–180 °C; ^{1}H NMR (DMSO-d_6) δ 9.31 (1H, s, N*H*NH$_2$), 7.69 (1H, s, 2-C*H*), 7.25–7.45 (4H, m, Ar*H*), 6.99 (1H, s, 4-C*H*), 4.59 (2H, s, NCH_2), 4.29 (2H, s, NHNH_2); ^{13}C NMR (DMSO-d_6) δ 166.4 (*C*=O), 160.6 (d, $^1J_{C,F}$ = 245 Hz, *para*-*C*F), 140.0 (2-*C*), 131.8 (5-*C*), 130.5 (d, $^3J_{C,F}$ = 8 Hz, *ortho*-*C*), 127.3 (4-C), 126.0 (d, $^4J_{C,F}$ = 3 Hz, 1′-*C*), 115.6 (d, $^2J_{C,F}$ = 22 Hz, *meta*-*C*), 45.8 (NCH$_2$); FTIR νmax/cm-1 (KBr): 3104, 3026, 2417, 1747, 1495, 1380, 1223, 1163, 1110, 928, 824, 698, 674, 544, HRMS (ESI-TOF) *m*/*z*: [M+H]$^+$ Calcd for $C_{11}H1_2FN_4O$ 235.0990, found 235.0995.

4.2.6.3. 2-(5-Phenyl-1H-imidazol-1-yl)acetohydrazide ***20b***. 2 Physical characteristics: pale yellow solid; Yields: 176 mg, 90%; Mp: 172–174 °C; ^{1}H NMR (DMSO-d_6) δ 9.32 (1H, s, N*H*NH$_2$), 7.36 (1H, s, 2-C*H*), 7.35–7.45 (5H, m, Ar*H*), 7.00 (1H, s, 4-C*H*), 4.62 (2H, s, NCH_2), 4.30 (2H, s, NHNH_2); ^{13}C NMR (DMSO-d_6) δ 167.5 (*C*=O), 141.1 (2-*C*), 133.2 (5-*C*), 130.5, 129.7, 129.1, 128.7, 128.1 (Ar*C*), 128.1 (4-*C*), 46.8 (NCH$_2$); FTIR νmax/cm-1 (KBr): 3321, 3197, 3119, 3026, 2950, 1676, 1638, 1608, 1553, 1489, 1425, 1298, 1285, 1229, 1112, 1006, 927, 909, 820, 767, 718, 703, 678, 647, 581, 534; HRMS (ESI (ESI-TOF) *m*/*z*: [M+H]$^+$ Calcd for $C_{11}H_{13}N_4O$ 217.1084, found 217.1082.

4.2.6.4. 2-[5-(3,5-Dimethoxyphenyl)-1H-imidazol-1-yl]acetohydrazide ***20c***. Physical characteristics: yellow solid; Yields: 259 mg,94%; Mp: 89–91 °C; ^{1}H NMR (DMSO-d_6) δ 9.37 (1H, s, N*H*NH$_2$), 7.66 (1H, s, 2-C*H*), 6.88–7.01 (4H, overlapping multiplets, Ar*H* and 4-C*H*), 4.59 (2H, s, NCH_2), 4.33 (2H, s, NHNH_2), 3.78 and 3.76 (6H, 2 x s, 2 x ArOCH_3); ^{13}C NMR (DMSO-d_6) δ 166.7 (*C*=O), 148.7 & 148.6 (2 x Ar*C*OCH$_3$), 139.6 (2-*C*), 132.8 (5-*C*), 126.5 (4-*C*), 121.9, 121.9, 111.9, 112.9 (Ar*C*), 55.5 and 55.4 (2 x ArCOCH$_3$), 45.8 (NCH$_2$); FTIR νmax/cm-1 (KBr): 3565, 3209, 2938, 2838, 1693, 1586, 1557, 1511, 1463, 1418, 1321, 1254, 1168, 1142, 1112, 1024, 868, 815, 766, 656, 628, 601, 534; HRMS (ESI-TOF) *m*/*z*: [M+H]$^+$ Calcd for $C_{13}H_{17}N_4O_3$ 277.1295, found 277.1260.

4.2.6.5. 2-(5-(Benzo[d][1,3]dioxol-6-yl)-1H-imidazol-1-yl)acetohydrazide ***20d***. Physical characteristics: pale yellow solid; Yields: 211 mg, 90%; Mp: 169–171 °C; ^{1}H NMR (DMSO-d_6) δ 9.33 (1H, s, N*H*NH$_2$), 7.65 (1H, s, 2-C*H*), 6.84–6.97 (4H, overlapping signals, Ar*H* and 4-C*H*), 6.06 (2H, s, ArOCH_2O), 4.58 (2H, s, NCH_2), 3.42 (2H, s, NHNH_2); ^{13}C NMR (DMSO-d_6) δ 170.9 (*C*=O), 147.5 and 147.1 (2 x Ar*C*OCH$_2$O), 139.6 (2-*C*), 132.7 (5-*C*), 127.2 (4-*C*), 126.7, 123.2, 122.0, 108.8 (Ar*C*), 101.3 (ArCOCH$_2$O), 45.7 (NCH$_2$); FTIR νmax/cm-1 (KBr): 3318, 3210, 3104, 2994, 2929, 1655, 1619, 1561, 1500, 1428, 1344, 1321, 1292, 1231, 1121, 1142, 1040, 968, 934, 918, 880, 874, 841, 833, 809, 759, 665, 642, 579; HRMS (ESI-TOF) *m*/*z*: [M+H]$^+$ Calcd. for $C_{12}H_{13}N_4O_3$ 261.0982, found 261.0992.

4.2.6.6. 2-[5-(4-tert-Butylphenyl)-1H-imidazol-1-yl]acetohydrazide ***20e***. Physical characteristics: pale yellow solid; Yields: 228 mg, 93%; Mp: 178–180 °C; ^{1}H NMR (DMSO-d_6) δ 9.36 (1H, s, N*H*NH$_2$), 7.69 (1H, s, 2-C*H*), 7.44 (2H, d, *J* = 8.0 Hz, Ar*H*), 7.31 (2H, d, *J* = 8.0 Hz, Ar*H*), 6.97 (1H, s, 4-C*H*), 4.61 (2H, s, NCH_2), 4.45 (2H, brs, NHNH_2), 1.30 [9H, s, C(CH_3)$_3$]; ^{13}C NMR (DMSO-d_6) δ 166.6 (*C*=O), 150.2 [Ar*C*C(CH$_3$)$_3$], 139.9 (2-*C*), 132.7, 127.9, 127.0, 126.7, 125.6 (Ar*C*), 45.8 (NCH$_2$), 34.4 [ArC*C*(CH$_3$)$_3$], 31.1 [ArCC(*C*H$_3$)$_3$]; FTIR νmax/cm-1 (KBr): 3335, 3220, 3062, 2957, 2865, 1663, 1603, 1589, 1501, 1478, 1382, 1362, 1296, 1274, 1228, 1116, 992, 964, 913, 842, 828, 783, 740,

648, 585, 564; HRMS (ESI-TOF) *m/z*: $[M+H]^+$ Calcd for $C_{15}H_{21}N_4O$ 273.1710, found 273.1727.

4.2.6.7. 2-(5-(3-Hydroxy-4-methoxyphenyl)-1H-imidazol-1-yl)acetohydrazide ***20f***. Physical characteristics: pale yellow solid; Yield: 222 mg, 94%; Mp: 217–219 °C; ^{1}H NMR (DMSO-d_6) δ 9.32 (1H, s, N*H*NH$_2$), 9.20 (1H, s, ArO*H*), 7.63 (1H, s, 2-C*H*), 6.75–7.69 (4H, overlapping signals, m, 4-C*H* and Ar*H*), 4.56 (2H, s, NC*H*$_2$)), 4.32 (2H, brs, NHN*H*$_2$), 3.36 (3H, s, ArOC*H*$_3$;^{13}C NMR (DMSO-d_6) δ 166.7 (*C*=O), 147.6 and 146.5 (ArCOCH$_3$ and ArCOH), 139.3 (2-*C*), 133.0 (5-*C*), 126.2, 121.2 (Ar*C*), 120.4 (4-*C*), 115.7, 112.4 (Ar*C*), 55.5 (ArCOCH$_3$), 46.9 (NCH$_2$); FTIR νmax/cm-1 (KBr): 3146, 3120, 3051, 2994, 2603, 1614, 1574, 1523, 1460, 1387, 1331, 1318, 1289, 1247, 1219, 1182, 1155, 1132, 1032, 857, 782, 673; HRMS (ESI-TOF) *m/z*: $[M+H]^+$ Calcd for $C_{12}H_{15}N_4O_3$ 263.1139, found 263.1145.

4.2.6.8. 2-[5-(3-Methoxyphenyl)-1H-imidazol-1-yl]acetohydrazide ***20g***. Physical characteristics: white solid; Yields: 191 mg, 86%; Mp: 152–154 °C; ^{1}H NMR (DMSO-d_6) δ 9.35 (1H, s, N*H*NH$_2$), 7.69 (1H, s, 2-C*H*), 7.32–7.36 (1H, m, Ar*H*), 7.02 (1H, s, 4-C*H*), 6.91–6.96 (3H, m, Ar*H*), 4.63 (2H, s, NC*H*$_2$), 4.31 (2H, s, NHN*H*$_2$) 3.77 (3H, s, ArOC*H*$_3$); ^{13}C NMR (DMSO-d_6) δ 166.5 (*C*=O), 159.4 (ArCOCH$_3$), 410.2 (2-*C*), 132.7 (5-*C*), 130.8, 129.9 (Ar*C*), 127.3 (4-*C*), 120.4, 113.7, 113.2 (Ar*C*), 55.1 (ArCOCH$_3$), 45.9 (NCH$_2$); FTIR νmax/cm-1 (KBr): 3320, 3198, 3012, 2954, 1677, 1606, 1589, 1563, 1493, 1482, 1473, 1425, 1319, 1293, 1250, 1218, 1118, 1113, 1030, 1008, 866, 849, 818, 797, 722, 700, 650, 574; HRMS (ESI-TOF) *m/z*: $[M+H]^+$ Calcd for $C_{12}H_{15}N_4O_2$ 247.1195, found 247.1208.

4.3. Biological studies

4.3.1. Indirect biochemical assays (ELISA and AlphaScreen™)

4.3.1.1. In vitro ELISA test for the binding of HIV-1 Vpu to BST-2. HIV-1 Vpu was overexpressed and purified using the protocol reported by Njengele et al. [71] The binding between HIV-1 Vpu and BST-2 was analysed using the enzyme-linked immunosorbent assay (ELISA) with the purified recombinant HIV-1 Vpu and a commercial BST-2 ELISA kit (Uscn Life Science). The assay was carried out according to the kit instructions, and all reagents used (with the exception of the HIV-1 Vpu) were provided with the kit. Briefly, 100 μL of BST-2, at a concentration of 5 ng/ml, was added on a 96-well microtiter plate that was pre-coated with an anti-BST-2 antibody. The plate was incubated at 37 °C for an hour, after which excess BST-2 was discarded and 100 μL of the recombinant HIV-1 Vpu was introduced at 5 and 10 ng/ml, respectively. The plate was incubated at 37 °C for another hour and 100 μL of a biotin-conjugated anti-BST-2 antibody at a dilution of 1:100 was subsequently added. Following another hour of incubation at 37 °C, 100 μL of Streptavidin conjugated to HRP was added and the plate was incubated at 37 °C for 30 min. The activity of the HRP enzyme was detected using the 3,3′,5,5′-Tetramethylbenzidine (TMB) substrate solution, and the enzyme-substrate reaction was terminated by the addition of 50 μL of the stop solution (10% sulfuric acid) 30 min after the addition of the substrate. The absorbance was measured spectrophotometrically at 450 nm.

4.3.1.2. Sandwich ELISA for compound screening. The ELISA test optimized above was used in the screening of the synthesized compounds that were identified to show inhibition against the HIV-1 Vpu/BST-2 interaction *in silico*. For this assay, 5 ng/ml of HIV-1 Vpu was incubated with 100 μM of each compound for 30 min at 37 °C with slight shaking, and 5 ng/ml of BST-2 was coated on a 96-well polysorp plate that was pre-coated with an anti-BST-2 antibody (Uscn Life Science). Following the incubation period, excess BST-2 was discarded and the HIV-1 Vpu/compound solutions were introduced at 100 μL. The plates were incubated at 37 °C for an hour, and a biotin-conjugated anti-BST-2 antibody (Uscn Life Science) was added and incubated at 37 °C for another hour. Streptavidin conjugated to HRP was added and the plates were incubated at 37 °C for 30 min. The activity of the HRP enzyme was detected as outlined above. The compounds were tested in duplicate wells and the assay was repeated three times. The inhibition percentage for each of the test compounds was calculated.

4.3.1.3. The HIV-1 Vpu/BST-2 AlphaScreen assay. An AlphaScreen assay was developed and used as a secondary screening assay to confirm the results obtained from the ELISA. The assay was performed using a biotinylated HIV-1 Vpu (tagged using a biotin labelling kit, Roche) and a commercial recombinant BST-2 protein with a Glutathione S-transferase (GST) tag (Abcam). HIV-1 Vpu and BST-2 were incubated together at a 1:1 ratio to a final concentration of 100 nM for each protein. Half-area Opti-Plates (PerkinElmer) were used and the proteins were diluted in an assay buffer composed of 25 mM HEPES (pH 7.4), 100 mM NaCl, and 0.1% BSA. Following a 2-h incubation of the proteins at 37 °C, Streptavidin Donor beads and anti-GST conjugated Acceptor beads (PerkinElmer) were added to a final concentration of 10 μg/ml. The plate was incubated at 30 °C in the dark for an hour and the luminescence response was subsequently read between 520 and 620 nm on the EnSpire Multimode plate reader (PerkinElmer). The following controls were included in the development of the assay: beads alone, HIV-1 Vpu alone, BST-2 alone, HIV-1 Vpu and BST-2 alone, and each protein with both beads.

To validate the compound screening results obtained from the ELISA, the AlphaScreen assay was used to confirm the activity of the compounds in inhibiting the HIV-1 Vpu/BST-2 interaction. For this assay, 400 nM of the biotinylated HIV-1 Vpu was incubated with 100 μM of each compound at 37 °C for 30 min. Following the incubation period, the recombinant GST-tagged BST-2 was added to a final concentration of 100 nM and incubated at 37 °C for an hour. Streptavidin Donor and anti-GST conjugated Acceptor beads were added at 10 μg/ml and the plate was incubated at 30 °C in the dark for an hour. The plate was read on the EnSpire Multimode plate reader as detailed above, and the inhibition percentages of the compounds were calculated. The compounds were tested in duplicate wells and the assays were repeated three times.

4.3.1.4. Dose-response studies in AlphaScreen™ assay. The optimized AlphaScreen assay from above was used to conduct dose-response studies for the compounds that showed the highest inhibition of the HIV-1 Vpu/BST-2 interaction. This was done to determine the concentrations of the compounds that caused 50% inhibition (IC_{50}) in the interaction. A total of eight serial dilutions ranging from 200 to 1.56 μM were run for each compound on this assay. Percentage inhibition was calculated for each concentration and plotted against the logarithm of the concentration. The compounds were tested in duplicate at each concentration and the assays were repeated three times. The obtained data was analysed and fitted using the Origin 6.0 software.

4.3.2. Cell-based assays

4.3.2.1. Cellular toxicity. The toxicity of the test compounds that showed activity in inhibiting the HIV-1 Vpu/BST-2 interaction against mammalian cells was evaluated using the 3-(4,5-dimethylthiazol-2-yl)-5-(3-carboxymethoxyphenyl)-2-(4-sulfophenyl)-2*H*-tetrazolium (MTS) cell proliferation assay according to the manufacturer. Briefly, MT-4 cells (NIH AIDS Reagents Programme, Division of AIDS, NIAID, NIH: catalogue number: 120) were seeded at a density of $1x10^5$ cells/mL and a final volume of 100 μL/well in 96-well cell culture plates (Sigma Aldrich). The cells were

incubated at 37 °C in a humidified atmosphere of 5% CO_2 for 4 h to allow for stabilization. Following the incubation period, dose-response studies of the test compounds were conducted using 2-fold serial dilutions, with final concentrations ranging from 200 to 1.56 μM in Roswell Park Memorial Institute (RPMI) 1640 medium (Gibco, Life Technologies) containing 10% (v/v) foetal calf serum (FCS, Highveld Biological). The plates were incubated under standard culture conditions (37 °C and 5% CO_2) for 72 h, after which the viability of the cells was determined using the MTS dye. The MTS solution, to a final volume of 20 μL per well, was added and the plates were incubated at 37 °C for an additional 4 h. The amount of soluble formazan produced was measured spectrophotometrically at 490 nm. Untreated MT-4 cells and Auranofin (Biomol International) were used as controls. The data was analysed using Origin 6.0 with the logarithmic value of each compound concentration plotted against the percentage of viable cells (%Viability) to obtain a dose-response curve. From the dose curve, a half-maximal cytotoxic concentration (CC_{50}) value for each compound was determined.

4.3.2.2. The antiviral activity of the compounds. The antiviral activity of the identified compounds against HIV-1 was investigated using MT-4 cells and the HIV-1 LAV viral strain. Briefly, MT-4 cells ($1x10^5$ cells/mL) were infected with the HIV-1 LAV at a multiplicity of infection (MOI) of 0.1. The virus-infected cells were plated onto 96-well tissue culture plates at 100 μL/well, and the plates were subsequently incubated at 37 °C in a humidified atmosphere of 5% CO_2 for 90 min. Following the incubation period, two-fold serial dilutions of each compound (200−1.56 μM) made up in 10% RPMI were added and the plates were incubated at 37 °C and 5% CO_2 for 72 h. The compounds were tested alongside HIV-1 infected cells without any compound treatment, as well as uninfected MT-4 cells as controls. Raltegravir, a known inhibitor of HIV-1, was used as a positive antiretroviral control. After the 72 h incubation, supernatants were collected from the cells and viral levels were analysed *via* a p24 ELISA test. Cell supernatants were used to test for the presence of the p24 antigen using the BioElisa HIV-1^{+2} Ag/AB kit (BIOKIT) according to the manufacturer's instructions. The data was used to determine the concentration of compound required to reduce the expression of p24, which is equivalent to viral replication, by 50% (EC_{50}). Selective activities of the compounds were calculated as follows:

Selectivity index (SI) = CC_{50} μM / IC_{50} (μM)

4.4. Aqueous solubility analysis of the compounds

To study the aqueous solubility of the identified inhibitors, a filtration-based assay that includes 96-well filter plates was adapted from Millipore and was conducted according to the manufacturer's instructions. Briefly, compound stocks were prepared in DMSO, and the standards were diluted in an 80:20 PBS: acetonitrile solution. The concentration of DMSO was maintained at 5% in all the standards, and standard concentrations of 500, 200, 50, 12.5 and 3.13 μM were prepared for the construction of a standard curve. The standards were incubated in a 96-well filter plate (Millipore, Merck) at room temperature shaking at 300 rpm overnight (~16 h). Following vacuum filtration, the compounds in solution were analysed *via* UV/Vis spectroscopy (measured from 200 to 800 nm at 10 nm increments). The inhibitors were tested alongside chloramphenicol as a positive control. Following the construction of the standard curves, 200 and 100 μM samples of the compounds were prepared in 100% PBS, incubated in a filter plate shaking overnight at room temperature. The plate was vacuum filtered and 80 μL of the compounds transferred to a UV-Star half-area microplate for analysis. A total of 20 μL acetonitrile was added per sample and the compounds were quantified using UV/Vis spectroscopy at the optimum wavelength for each compound. The amount of soluble compound in the aqueous sample was quantified using the following equation:

Aqueous Solubility = (Amax Filtrate/ Slope) * 1.25

Where the maximum absorbance of each compound (***Amax***) was divided by the slope of the line from the respective calibration curve and multiplied by a factor of 1.25 to account the dilution with acetonitrile.

4.5. In silico assessment of the physicochemical properties of the compounds

4.5.1. Ligand preparation

Prior to the prediction of physicochemical properties, the selected compounds were energy minimized using a CHARMM based force field function under Small Molecules' Prepare and Filter Ligands function to generate all possible combinations of stereoisomers and conformers [68].

4.5.2. Prediction of drug-likeness of compounds

The compounds that showed good inhibition percentages for the HIV-1 Vpu/BST-2 interaction were analysed for drug-likeness according to Lipinski's rule-of-five. For a compound to be considered as a potential 'lead', it should exhibit specific binding towards the target and the absorption, distribution, metabolism, excretion and toxicity (ADME-T) properties of the compound should be known. The rule-of-five predicts that poor absorption is more likely when a compound has a molecular mass greater than 500 g/mol, has more than 10 hydrogen bond acceptors (N and O atoms), more than 5 hydrogen bond donors (OH and NH groups) and has an octanol-water partition coefficient (LogP) value of more than 5 [67,72]. The water-octanol partitioning co-efficiency (LogP), as well as the number of hydrogen bond donors and acceptors in each compound were determined using the Biovia Discovery Studio ™ software package.

Declaration of competing interest

The authors declare that they have no known competing financial interests or personal relationships that could have appeared to influence the work reported in this paper.

Acknowledgements

We acknowledge with thanks financial support from the National Research Foundation Professional Development Program (UID: 78999) of South Africa and NRF Thuthuka grant (UID: 117794), The South African Medical Research Council (grant number: 82760), Mintek and the University of the Witwatersrand.

Appendix A. Supplementary data

Supplementary data to this article can be found online at https://doi.org/10.1016/j.ejmech.2020.112111.

References

[1] F. Clavel, A.J. Hance, HIV drug resistance, N. Engl. J. Med. 350 (2004) 1023−1035, https://doi.org/10.1056/NEJMra025195.

[2] M. Zazzi, H. Hu, M. Prosperi, The global burden of HIV-1 drug resistance in the past 20 years, Peer J 6 (2018) 1–16, https://doi.org/10.7717/peerj.4848, e4848.

[3] HIV Drug Resistance Report 2019, World Health Organization, Geneva, Switzerland, 2019 (WHO/CDS/HIV/19.21). Licence: CC BY-NC-SA 3.0 IGO, https://apps.who.int/iris.

[4] O. Taltynov, B.A. Desimmie, J. Demeulemeester, F. Christ, Z. Debyser, Cellular cofactors of lentiviral integrase: from target validation to drug discovery, Mol. Biol. Int. 863405 (2012) 1–16, https://doi.org/10.1155/2012/863405.

[5] Y.-M. Tzou, R. Shin, N.R. Krishna, HIV-1 virus interactions with host proteins: interaction of the N-terminal domain of the HIV-1 capsid protein with human calmodulin, Nat. Prod. Commun. 14 (5) (2019) 1–11, https://doi.org/10.1177/1934578X19849190.

[6] W. Fu, B.E. Sanders-Beer, K.S. Katz, D.R. Maglott, K.D. Pruitt, R.G. Ptak, Human immunodeficiency virus type 1, human protein interaction database at NCBI, Nucleic Acids Res. 37 (2009) D417–D422, https://doi.org/10.1093/nar/gkn708.

[7] B. Mangeat, G. Gers-Huber, M. Lehmann, M. Zufferey, J. Luban, V. Piguet, HIV-1 vpu neutralizes the antiviral factor tetherin/BST-2 by binding it and directing its beta-TrCP2-dependent degradation, PLoS Pathog. 5 (9) (2009), e1000574, https://doi.org/10.1371/journal.ppat.1000574.

[8] F.M. Pujol, V. Laketa, F. Schmidt, M. Mukenhirn, B. Müller, S. Boulant, D. Grimm, O.T. Keppler, O.T. Fackler, HIV-1 Vpu antagonizes CD317/tetherin by adaptor protein-1-mediated exclusion from virus assembly sites, J. Virol. 90 (15) (2016) 6709–6723, https://doi.org/10.1128/JVI.00504-16.

[9] R.S. Harris, J.F. Hultquist, D.T. Evans, The restriction factors of human immunodeficiency virus, J. Biol. Chem. 287 (49) (2012) 40875–40883. https://dx.doi.org/10.1074/jbc.R112.416925.

[10] S.J. Neil, T. Zang, P.D. Bieniasz, Tetherin inhibits retrovirus release and is antagonized by HIV-1 Vpu, Nature 451 (2008) 425–430. https://dx.doi.org/10.1038/nature06553.

[11] J.F. Arias, Y. Iwabu, K. Tokunaga, Structural basis for the antiviral activity of BST-2/tetherin and its viral antagonism, Front. Microbiol. 250 (2011) 1–9, https://doi.org/10.3389/fmicb.2011.00250.

[12] J. Ishikawa, T. Kaisho, H. Tomizawa, B.O. Lee, Y. Kobune, J. Inazawa, K. Oritani, M. Itoh, T. Ochi, K. Ishihara, T. Hirano, Molecular cloning and chromosomal mapping of a bone marrow stromal cell surface gene, BST2, that may be involved in pre-B-cell growth, Genomics 26 (1995) 527–534, https://doi.org/10.1016/0888-7543(95)80171-H.

[13] S. Kupzig, V. Korolchuk, R. Rollason, A. Sugden, A. Wilde, G. Banting, Bst-2/HM1.24 is a raft-associated apical membrane protein with an unusual topology, Traffic 4 (2003) 694–709, https://doi.org/10.1034/j.1600-0854.2003.00129.x.

[14] E.A. Cohen, E.F. Terwilliger, J.G. Sodroski, W.A. Haseltine, Identification of a protein encoded by the vpu gene of HIV-1, Nature 334 (6182) (1988) 532–534, https://doi.org/10.1038/334532a0.

[15] K. Strebel, T. Klimkait, M.A. Martin, A novel gene of HIV-1, vpu, and its 16-kilodalton product, Science 241 (4870) (1988) 1221–1223, https://doi.org/10.1126/science.3261888.

[16] J.G. Magadán, J.S. Bonifacino, Transmembrane domain determinants of CD4 downregulation by HIV-1 vpu, J. Virol. 86 (2) (2012) 757–772, https://doi.org/10.1128/JVI.05933-11.

[17] U. Schubert, S. Bour, A.V. Ferrer-Montiel, M. Montal, F. Maldarell, The two biological activities of human immunodeficiency virus type 1 Vpu protein involve two separable structural domains, J. Virol. 70 (1996) 809–819. PMID: 8551619; PMCID: PMC189883.

[18] T. Federau, U. Schubert, J.O.S.E.F. Floßdorf, P. Henklein, D. Schomburg, V. Wray, Solution structure of the cytoplasmic domain of the human immunodeficiency virus type 1 encoded virus protein U (Vpu), Int. J. Pept. Protein Res. 47 (4) (1996) 297–310, https://doi.org/10.1111/j.1399-3011.1996.tb01359.x.

[19] E. Pacyniak, M.L. Gomez, L.M. Gomez, E.R. Mulcahy, M. Jackson, D.R. Hout, B.J. Wisdom, E.B. Stephens, Identification of a region within the cytoplasmic domain of the subtype B Vpu protein of human immunodeficiency virus type 1 (HIV-1) that is responsible for retention in the golgi complex and its absence in the Vpu protein from a subtype C HIV-1, AIDS Res. Hum. Retrovir. 21 (5) (2005) 379–394, https://doi.org/10.1089/aid.2005.21.379.

[20] T. Klimkait, K. Strebel, M.D. Hoggan, M.A. Martin, J.M. Orenstein, The human immunodeficiency virus type 1-specific protein vpu is required for efficient virus maturation and release, J. Virol. 64 (2) (1990) 621–629. PMID: 2404139 PMCID: PMC249152.

[21] E.F. Terwilliger, E.A. Cohen, Y.C. Lu, J.G. Sodroski, W.A. Haseltine, Functional role of human immunodeficiency virus type 1 vpu, Proc. Natl. Acad. Sci. Unit. States Am. 86 (13) (1989) 5163–5167, https://doi.org/10.1073/pnas.86.13.5163.

[22] A. Andrew, K. Strebel, HIV-1 Vpu targets cell surface markers CD4 and BST-2 through distinct mechanisms, Mol. Aspect. Med. 31 (5) (2010) 407–417, https://doi.org/10.1016/j.mam.2010.08.002.

[23] J.L. Douglas, K. Viswanathan, M.N. McCarroll, J.K. Gustin, K. Früh, A.V. Moses, Vpu directs the degradation of the human immunodeficiency virus restriction factor BST-2/Tetherin via a βTrCP-dependent mechanism, J. Virol. 83 (16) (2009) 7931–7947, https://doi.org/10.1128/JVI.00242-09.

[24] M. Dubé, B.B. Roy, P. Guiot-Guillain, J. Binette, J. Mercier, A. Chiasson, É.A. Cohen, Antagonism of tetherin restriction of HIV-1 release by Vpu involves binding and sequestration of the restriction factor in a perinuclear compartment, PLoS Pathog. 6 (4) (2010a), e1000856, https://doi.org/10.1371/journal.ppat.1000856.

[25] M. Dubé, M.G. Bego, C. Paquay, É.A. Cohen, Modulation of HIV-1-host interaction: role of the Vpu accessory protein, Retrovirology 7 (1) (2010b) 114, https://doi.org/10.1186/1742-4690-7-114.

[26] Y. Iwabu, H. Fujita, M. Kinomoto, K. Kaneko, Y. Ishizaka, Y. Tanaka, T. Sata, K. Tokunaga, HIV-1 accessory protein Vpu internalizes cell-surface BST-2/tetherin through transmembrane interactions leading to lysosomes, J. Biol. Chem. J. Biol. Chem. 284 (2009) 35060–35072, https://doi.org/10.1074/jbc.M109.058305.

[27] R.K. Gupta, S. Hue, T. Schaller, E. Verschoor, D. Pillay, G.J. Towers, Mutation of a single residue renders human tetherin resistant to HIV-1 Vpu-mediated depletion, PLoS Pathog. 5 (2009), e1000443, https://doi.org/10.1371/journal.ppat.1000443.

[28] M. Skasko, Y. Wang, Y. Tian, A. Tokarev, J. Munguia, A. Ruiz, E.B. Stephens, S.J. Opella, J. Guatelli, HIV-1 Vpu protein antagonizes innate restriction factor BST-2 via lipid-embedded helix-helix interactions, J. Biol. Chem. 287 (1) (2012) 58–67, https://doi.org/10.1074/jbc.M111.296772.

[29] Z. Mi, X. Wang, Y. He, X. Li, J. Ding, H. Liu, J. Zhou, S. Cen, A novel peptide to disrupt the interaction of BST-2 and Vpu, Biopolymers 102 (3) (2014) 280–287, https://doi.org/10.1002/bip.22488.

[30] G. Khoury, G. Ewart, C. Luscombe, M. Miller, J. Wilkinson, Antiviral efficacy of the novel compound BIT225 against HIV-1 release from human macrophages, Antimicrob. Agents Chemother. 54 (2) (2010) 835–845, https://doi.org/10.1128/AAC.01308-09.

[31] Q. Zhang, Z. Mi, Y. Huang, L. Ma, J. Ding, J. Wang, Y. Zhang, Y. Chen, J. Zhou, F. Guo, X. Li, S. Cen, 2-thio-6-azauridine inhibits Vpu mediated BST-2 degradation, Retrovirology 2 (13) (2016) 13, https://doi.org/10.1186/s12977-016-0247-z.

[32] P. Mwimanzi, I. Tietjen, S.C. Miller, A. Shahid, K. Cobarrubias, N.N. Kinloch, B. Baraki, J. Richard, A. Finzi, D. Fedida, Z.L. Brumme, M.A. Brockman, Novel acylguanidine-based inhibitor of HIV-1, J. Virol. 90 (20) (2016) 9495–9508, https://doi.org/10.1128/JVI.01107-16.

[33] Z. Mi, J. Ding, Q. Zhang, J. Zhou, L. Ma, H. Yu, Z. Liu, G. Shan, X. Li, J. Zhou, T. Wei, L. Zhang, F. Guo, C. Liang, S. Cen, A small molecule compound IMB-LA inhibits HIV-1 infection by preventing viral Vpu from antagonizing the host restriction factor BST-2, Sci. Rep. 6 (5) (2015), https://doi.org/10.1038/srep18499, 18499: 1-18.

[34] S.M. King, S.L. Buchwald, Development of a method for the *N*-arylation of amino acid esters with aryl triflates, Org. Lett. 18 (2016) 4128–4141, https://doi.org/10.1021/acs.orglett.6b02082.

[35] Y. Farhadi, S.N.R. Hashemian, Computer-aided design of amino acid-based therapeutics: a review, Drug Des. Dev. Ther. 12 (2018) 1239–1254, https://doi.org/10.2147/DDDT.S159767.

[36] M.A. Blaskovish, Unusual amino acids in medicinal chemistry, J. Med. Chem. 59 (24) (2016) 10807–10836, https://doi.org/10.1021/acs.jmedchem.6b00319.

[37] M. Hammond, J.R. Patterson, S. Manns, T.H. Hoang, D.G. Washburn, W. Trizna, L. Glace, E.T. Grygielko, R. Nagilla, M. Nord, H.E. Fries, D.J. Minick, N.J. Laping, J.D. Bray, S.K. Thompson, Synthesis and SAR of amino acid-derived heterocyclic progesterone receptorfull and partial agonists *Bioorg*, Med. Chem. Lett. 19 (2009) 2637–2641, https://doi.org/10.1016/j.bmcl.2009.03.146.

[38] T. Farhadi, N. Nezafat, Y. Ghasemi, Z. Karimi, S. Hemmati, N. Erfani, Designing of complex multi-epitope peptide vaccine based on Omps of Klebsiella pneumoniae: an in silico approach, Int. J. Pept. Res. Therapeut. 21 (3) (2015) 325–341, https://doi.org/10.1007/s10989-015-9461-0.

[39] J.-C. Xiang, Z.-X. Wang, Y. Cheng, S.-H. Xia, M. Wang, B.-C. Tang, Y.-D. Wu, A.-X. Wu, Divergent synthesis of functionalized quinolines from aniline and two distinct amino acids, J. Org. Chem. 82 (17) (2017) 9210–9216, https://doi.org/10.1021/acs.joc.7b0150.

[40] S.H. Bae, J.H. Park, H.G. Choi, H. Ki, S.H. Kim, Imidazole antifungal drugs inhibit the cell proliferation and invasion of human breast cancer cells, Biomolecules and Therapeutics 26 (5) (2018) 494–502, https://doi.org/10.4062/biomolther.2018.042.

[41] N. Rani, A. Sharma, G.K. Gupta, R. Singh, Imidazoles as potential antifungal agents: a review, Mini Rev. Med. Chem. 13 (11) (2013) 1626–1655, https://doi.org/10.2174/13895575113139990069.

[42] E. Serrao, Z.-L. Xu, B. Debnath, F. Christ, Z. Debyser, Y.-Q. Long, N. Neamati, Discovery of a novel 5-carbonyl-1*H*-imidazole-4-carboxamide class of inhibitors of the HIV-1 integrase-LEDGF/p75 interaction, Bioorg. Med. Chem. 21 (2013) 5963–5972, https://doi.org/10.1016/j.bmc.2013.07.047.

[43] R. Singh, S. Ganguly, Design, synthesis and evaluation of some novel 1-phenyl-3-(5-phenyl-1*H*-imidazol-1-yl) thiourea derivatives as anti-HIV agents, Indian J Pharm Educ 52 (4) (2018) 655–665, https://doi.org/10.5530/ijper.52.4.76.

[44] R.V. Shingalapur, K.M. Hosamani, R.S. Keri, Synthesis and evaluation of in vitro anti-microbial and anti-tubercular activity of 2-styryl benzimidazoles, Eur. J. Med. Chem. 44 (2009) 4244–4248, https://doi.org/10.1016/j.ejmech.2009.05.021.

[45] D. Sharma, B. Narasimhan, P. Kumar, V. Judge, R. Narang, E. De Clercq, J. Balzarini, Synthesis, antimicrobial and antiviral evaluation of substituted imidazole derivatives, Eur. J. Med. Chem. 44 (2009) 2347–2353, https://doi.org/10.1016/j.ejmech.2008.08.010.

[46] H.-S. Kim, J.R. Jadhav, S.-J. Jung, J.-H. Kwak, Synthesis and antimicrobial activity of imidazole and pyridine appended cholestane-based conjugates, Bioorg. Med. Chem. Lett 23 (2013) 4315–4318, https://doi.org/10.1016/j.bmcl.2013.05.098.

[47] I. Ali, M.N. Lone, H.Y. Aboul-enein, Imidazoles as potential anticancer agents, Med Chem Comm 8 (2017), https://doi.org/10.1039/C7MD00067G, 1742-177.

[48] A.M. Van Leusen, B.E. Hoogenboom, H. Sierius, A novel and efficient synthesis of oxazoles from tosylmethylisocyanide and carbonyl compounds, Tetrahedron Lett. 13 (1972) 3114–3118, https://doi.org/10.1016/S0040-4039(01)85305-3.
[49] D. Van Leusen, E. van Echten, A.M. Van Leusen, Chemistry of sulfonylmethyl isocyanides. 37. Synthesis of 3,4-disubstituted pyrroles bearing substituents of electron-withdrawing and/or electron-donating nature, J. Org. Chem. 57 (1992) 2245–2249, https://doi.org/10.1021/jo00034a011.
[50] A.D. Mathiyazhagan, G. Anilkumar, Recent advances and applications of *p*-toluenesulfonylmethyl isocyanide (TosMIC), Org. Biomol. Chem. 17 (2019) 6735–6747, https://doi.org/10.1039/C9OB00847K.
[51] C.S. Shantharam, D.M. Suyoga Vardhan, R. Suhas, D.C. Gowda, Design and synthesis of amino acids conjugated heterocycle derived ureas/thioureas as potent inhibitors of protein glycation, Russ. J. Bioorg. Chem. 40 (2014) 443–454, https://doi.org/10.1134/S1068162014040128.
[52] M. Wang, K.P. Rakesh, J. Leng, W.-N. Fang, L. Ravindar, D.C. Gowda, H.-L. Qin, Amino acids/peptides conjugated heterocycles: a tool for the recent development of novel therapeutic agents, Bioogr. Chem. 76 (2018) 113–129, https://doi.org/10.1016/j.bioorg.2017.11.007.
[53] Y. Jin, M. Jiang, H. Wang, H. Fu, Installing amino acids and peptides on N-heterocycles under visible light assistance, Sci. Rep. 6 (2006) 20068, https://doi.org/10.1038/srep20068.
[54] K.C. Prakasha, G.M. Raghavendra, R. Harisha, D.C. Gowda, Design, synthesis and antimicrobial screening of amino acids conjugated 2-amino-4-arylthiazole derivatives, Int. J. Pharm. Pharmaceut. Sci. 3 (2011) 120–125.
[55] T.J. Rashamuse, A.T. Harrison, S. Mosebi, S. van Vuuren, E.M. Coyanis, M.L. Bode, Design, synthesis and biological evaluation of imidazole and oxazole fragments as HIV-1 integrase-LEDGF/p75 disruptors and inhibitors of microbial pathogens, Bioorg. Med. Chem. 28 (2020) 115210, https://doi.org/10.1016/j.bmc.2019.115210.
[56] M.L. Bode, D. Gravestock, A.L. Rousseau, Synthesis, uses and reactions of isocyanides in organic synthesis. An update, Org. Prep. Proced. Int. 48 (2016) 89–221, https://doi.org/10.1080/00304948.2016.1138072.
[57] M.J. O'Donnell, W.D. Bennett, W.A. Bruder, W.N. Jacobsen, K. Knuth, B. LeClef, R.L. Polt, F.G. Bordwell, S.R. Mrozack, T.A. Cripe, Acidities of glycine Schiff bases and alkylation of their conjugate bases, J. Am. Chem. Soc. 110 (1988) 8520–8525, https://doi.org/10.1021/ja00233a031.
[58] R. De Wachter, L. Brans, S. Ballet, I. Van den Eynde, D. Feytens, A. Keresztes, G. Toth, Z. Urbanczyk-Lipkowska, D. Tourwé, Influence of ring substitution on the conformation and β-turn mimicry of 4-amino-1,2,4,5-tetrahydro-2-benzazepin-3-one peptide mimetics, Tetrahedron 65 (2009) 2266–2278, https://doi.org/10.1016/j.tet.2009.01.057.
[59] O.I. Shamtova, N.E. Shevchenko, E.S. Balenkova, G.-V. Röschenthaler, V.G. Nenajdenko, Friedel–Crafts alkylation of natural amino acid-derived pyrroles with CF3-substituted cyclic imines, Mendeleev Commun. 23 (2013) 92–93, https://doi.org/10.1016/j.mencom.2013.03.013.
[60] T.J. Rashamuse, R. Klein, P.T. Kaye, Synthesis of Baylis-Hillman-Derived phosphonated 3-(benzylaminomethyl)-coumarins, Synth. Commun. 40 (2010) 3683–3690, https://doi.org/10.1080/00397910903531649.
[61] J.H. Frank, Y.L. Powder-George, R.S. Ramsewak, W.F. Reynolds, Variable-temperature ^{1}H-NMR studies on two C-glycosylflavones, Molecules 17 (2012) 7914–7926, https://doi.org/10.3390/molecules17077914.
[62] A. Voller, A. Barlet, D.E. Bidwell, Enzyme immunoassays with special reference to ELISA techniques, J. Clin. Pathol. 31 (6) (1978) 507–520, https://doi.org/10.1136/jcp.31.6.507.
[63] L. Beaudet, R. Rodriguez-Suarez, M.-H. Venne, M. Caron, J. Bédard, V. Brechler, S. Parent, M. Bielefeld-Sévigny, AlphaLISA immunoassays: the no-wash alternative to ELISAs for research and drug discovery, Nat. Methods 5 (2008) A10–A11, https://doi.org/10.1038/nmeth.f.230.
[64] M.B. Harbut, C. Vilchèze, X. Luo, M.E. Hensler, H. Guo, B. Yang, A.K. Chatterjee, V. Nizet, W.R. Jacobs, P.G. Schultz, F. Wang, Auranofin exerts broad-spectrum bactericidal activities by targeting thiol-redox homeostasis, Proc. Natl. Acad. Sci. U. S. A. 112 (14) (2015) 4453–4458, https://doi.org/10.1073/pnas.1504022112.
[65] A. Heredia, S. Hassounah, S. Medina-Moreno, J.C. Zapata, N.M. Le, Y. Han, J.S. Foulke Jr., C. Davis, J. Bryant, R.R. Redfield, M.A. Wainberg, Monotherapy with either dolutegravir or raltegravir fails to durably suppress HIV viraemia in humanized mice, J. Antimicrob. Chemother. 72 (9) (2017) 2570–2573, https://doi.org/10.1093/jac/dkx195.
[66] M.C. Rogge, D.R. Taft, Preclinical Drug Development, second ed., In- forma Healthcare USA, Inc., New York, 2010, p. 187. D.A.T.P. Sciences.
[67] C.A. Lipinski, F. Lombardo, B.W. Dominy, P. Feeney, Experimental and computational approaches to estimate solubility and permeability in drug discovery and development settings, J. Adv. Drug. Delivery. Rev. 23 (1997) 3–25, https://doi.org/10.1016/S0169-409X(96)00423-1.
[68] Dassault Systèmes Biovia, BIOVIA Workbook, Release 2017; BIOVIA Pipeline Pilot, Release 2017, Dassault Systèmes, San Diego, 2017.
[69] R.W. Chambers, F.H. Carpenter, The preparation and properties of some amino acid amides, J. Am. Chem. Soc. 77 (1955) 1522–1526, https://doi.org/10.1021/ja01611a036.
[70] S.J. Lee, E. Kim, M.L. Seo, Y. Do, Y.-A. Lee, S.S. Lee, J.H. Jung, M. Kogiso, T. Shimizu, Self-assembled helical ribbon and tubes of alanine-based amphiphiles induced by two different formation mechanisms, Tetrahedron 64 (2008) 1301–1308, https://doi.org/10.1016/j.tet.2007.11.062.
[71] Z. Njengele, R. Kleynhans, Y. Sayed, S. Mosebi, Expression, purification and characterization of a full-length recombinant HIV-1 Vpu from inclusion bodies, Protein Expr. Purif. 128 (2016) 109–114, https://doi.org/10.1016/j.pep.2016.08.018.
[72] T. Wunberg, M. Hendrix, A. Hillisch, M. Lobell, H. Meier, C. Schmeck, H. Wild, B. Hinzen, Improving the hit-to-lead process: data-driven assessment of drug-like and lead-like screening hits, Drug Discov. Today 11 (2006) 175–178, https://doi.org/10.1016/S1359-6446(05)037.